ELSEVIER

Contents lists available at ScienceDirect

Journal of Cleaner Production

journal homepage: www.elsevier.com/locate/jclepro





DISPLACE post-combustion carbon capture technology - Integration in a steel plant for mitigation of CO_2 emissions

Nicola Zecca ^a, Leonie Lücking ^{b,*}, Dora-Andreea Chisăliță ^b, Jurriaan Boon ^b, H.A.J. van Dijk ^b, J.A.Z. Pieterse ^b, Antonio Giuffrida ^a, Giampaolo Manzolini ^a

ARTICLE INFO

Handling Editor: Yutao Wang

Keywords:
Steel
BF-BOF
DISPLACE
CCUS
CO₂ mitigation
Post-combustion CC
Adsorption separation

ABSTRACT

The decarbonization of the steel industry, responsible for approximately 7% of global direct energy-related CO_2 emissions, is pivotal in advancing toward a more sustainable future. Carbon capture technologies play a crucial role in achieving this objective. This study presents the description, modelling, and characterization of the DISPLACE carbon capture technology, an isothermal and isobaric adsorption technology using with concentration swing regeneration. The process yields a high-purity CO_2 stream alongside a CO_2 -lean gas stream and its application to the decarbonization of flue gas from oxy-fired hot-stoves in a BF-BOF steel mill is described. Various DISPLACE operating conditions were simulated reaching performances of carbon capture ratios up to 98% and (dry) carbon purities up to 99%. Environmental and economic Key Performance Indicators (KPIs) were assessed, demonstrating the advantage of operating at 400 °C due to the reduced DISPLACE steam-to-carbon ratio. The production of steam for adsorbent regeneration requires additional fuel such as NG or coke oven gas (COG). When operating DISPLACE at optimal conditions and considering COG as fuel, a carbon avoidance greater than 78% can be reached with a SPECCA and a CCA equal to 3.65 GJ/ t_{CO2} and 91.89 ϵ / t_{CO2} respectively, values significantly lower than competitive MEA technology (SPECCA equal to 4.86 GJ/ t_{CO2} and CCA of 113.33 ϵ / t_{CO2}). Additionally, the impact of varying DISPLACE carbon capture ratios (CCR) and carbon purity was evaluated.

Nomenclature

Acronyms	
BF	Blast Furnace
BFG	Blast Furnace Gas
BOF	Basic Oxygen Furnace
BOFG	Basic Oxygen Furnace Gas
CCA	Cost of CO ₂ Avoided [€/t _{CO2}]
CCR	CO ₂ Capture Ratio
CCS	Carbon Capture and Storage
Co	Contingencies [€]
COG	Coke Oven Gas
EPC	Engineering, Procurement and Construction $[\epsilon]$
FCF	Fixed Charge Factor
GHG	Greenhouse Gases
HRC	Hot Rolled Coil
LCOHRC	Levelized Cost Of HRC
MEA	Monoethanolamine
NG	Natural Gas
	(continued on next column)

⁽continued)

PEC Primary Energy Consumption $[GJ/t_{product}]$ SEWGS Sorption Enhanced Water Gas Shift SPECCA Specific PEC for CO_2 Avoided $[GJ/t_{CO2}]$ TDPC Total Direct Plant Cost $[\mathfrak{E}]$ TAC Total Annualised Cost $[M\mathfrak{E}/y]$ TEC Total Equipment Cost $[\mathfrak{E}]$ TIC Total Installation Cost $[\mathfrak{E}]$ TPC Total Plant Cost $[\mathfrak{E}]$ Greek	OC	Owner's cost [€]
$\begin{array}{llll} \text{SPECCA} & \text{Specific PEC for CO}_2 \text{Avoided [GJ/t}_{\text{CO2}}] \\ \text{TDPC} & \text{Total Direct Plant Cost } [\ell] \\ \text{TAC} & \text{Total Annualised Cost } [\mathbb{M}^\ell/y] \\ \text{TEC} & \text{Total Equipment Cost } [\ell] \\ \text{TIC} & \text{Total Installation Cost } [\ell] \\ \text{TPC} & \text{Total Plant Cost } [\ell] \\ \end{array}$	PEC	Primary Energy Consumption [GJ/t _{product}]
TDPC Total Direct Plant Cost $[\mathfrak{E}]$ TAC Total Annualised Cost $[\mathfrak{M}\mathfrak{E}/y]$ TEC Total Equipment Cost $[\mathfrak{E}]$ TIC Total Installation Cost $[\mathfrak{E}]$ TPC Total Plant Cost $[\mathfrak{E}]$ Greek ϵ_b Bed porosity $[\cdot]$ η Efficiency $[\cdot]$ ρ Gas density $[kg/m^3]$ τ Plant availability $[\cdot]$ ω Mass fraction $[\cdot]$	SEWGS	Sorption Enhanced Water Gas Shift
$ \begin{array}{cccccccccccccccccccccccccccccccccccc$	SPECCA	Specific PEC for CO ₂ Avoided [GJ/t _{CO2}]
TEC Total Equipment Cost $[\mathfrak{E}]$ TIC Total Installation Cost $[\mathfrak{E}]$ TPC Total Plant Cost $[\mathfrak{E}]$ Greek \mathfrak{E}_b Bed porosity $[\cdot]$ \mathfrak{p} Efficiency $[\cdot]$ \mathfrak{p} Gas density $[kg/m^3]$ \mathfrak{r} Plant availability $[\cdot]$ \mathfrak{w} Mass fraction $[\cdot]$	TDPC	Total Direct Plant Cost [€]
TIC Total Installation Cost $[\mathfrak{E}]$ TPC Total Plant Cost $[\mathfrak{E}]$ Greek \mathfrak{E}_{b} Bed porosity $[\cdot]$ \mathfrak{p} Efficiency $[\cdot]$ \mathfrak{p} Gas density $[kg/m^{3}]$ \mathfrak{r} Plant availability $[\cdot]$ \mathfrak{w} Mass fraction $[\cdot]$	TAC	Total Annualised Cost [M€/y]
TPC Total Plant Cost $[\mathfrak{E}]$ Greek ϵ_b Bed porosity $[\cdot]$ ρ Efficiency $[\cdot]$ ρ Gas density $[kg/m^3]$ τ Plant availability $[\cdot]$ ω Mass fraction $[\cdot]$	TEC	Total Equipment Cost [€]
$\begin{array}{lll} \text{Greek} & & & & \\ \varepsilon_b & & & \text{Bed porosity [-]} \\ \eta & & & \text{Efficiency [-]} \\ \rho & & & \text{Gas density [kg/m}^3] \\ \tau & & & \text{Plant availability [-]} \\ \omega & & & \text{Mass fraction [-]} \\ \end{array}$	TIC	Total Installation Cost [€]
$\begin{array}{lll} \varepsilon_b & & \text{Bed porosity [-]} \\ \eta & & \text{Efficiency [-]} \\ \rho & & \text{Gas density [kg/m}^3] \\ \tau & & \text{Plant availability [-]} \\ \omega & & \text{Mass fraction [-]} \end{array}$	TPC	Total Plant Cost [€]
$\begin{array}{lll} \varepsilon_b & & \text{Bed porosity [-]} \\ \eta & & \text{Efficiency [-]} \\ \rho & & \text{Gas density [kg/m}^3] \\ \tau & & \text{Plant availability [-]} \\ \omega & & \text{Mass fraction [-]} \end{array}$		
η Efficiency [-] $ρ$ Gas density [kg/m ³] $τ$ Plant availability [-] $ω$ Mass fraction [-]	Greek	
ρ Gas density [kg/m³] τ Plant availability [-] ω Mass fraction [-]	$\epsilon_{ m b}$	Bed porosity [-]
τ Plant availability [-] ω Mass fraction [-]	η	Efficiency [-]
ω Mass fraction [-]	ρ	Gas density [kg/m³]
	τ	Plant availability [-]
Symbols	ω	Mass fraction [-]
	Symbols	

(continued on next page)

E-mail address: leonie.lucking@tno.nl (L. Lücking).

https://doi.org/10.1016/j.jclepro.2025.144739

Received 7 June 2024; Received in revised form 15 November 2024; Accepted 9 January 2025 Available online 10 January 2025

0959-6526/© 2025 The Authors. Published by Elsevier Ltd. This is an open access article under the CC BY-NC-ND license (http://creativecommons.org/licenses/by-nc-nd/4.0/).

^a Politecnico di Milano, Dipartimento di Energia, Via Lambruschini 4, 20126, Milano, Italy

^b TNO, Westerduinweg 3, 1755 LE, Petten, the Netherlands

^{*} Corresponding author.

(continued)

(continued)	
a_P	Particle interfacial area per unit volume [1/m]
c	Molar concentration [mol/m ³]
C_0	Reference cost
C_{f}	Fixed Costs [M€/y]
C_{v}	Variable Costs [M€/y]
$d_{ m p}$	Particle diameter [m]
D_z	Axial mass dispersion coefficient [m ² /s]
e_{CO2}	Specific CO ₂ emissions [t _{CO2} /t _{product}]
f	Friction factor [-]
$k_{ m LDF}$	Linear driving force coefficient [1/s]
M	Molar mass [kg/mol]
m	Mass flowrate [kg/s]
m _{sorbent}	Sorbent mass [kg]
N	Molar flux [mol/m ² s]
ń	Molar flowrate [mol/s]
n	Plant lifetime [years]
p	Pressure [Pa]
r	Interest rate [%]
S_0	Reference size
ΔT	Temperature difference [°C]
t	Time [s]
u	Superficial gas velocity [m/s]
v	Interstitial gas velocity [m/s]
Subscripts	
e	Electric
i	Species index
int	interphase
h	Hydraulic
m	Mechanical
p	Polytropic

1. Introduction

In accordance with the Paris Agreement, CO₂ emissions to the atmosphere must be strongly reduced. This is especially difficult for industries that have CO₂ emissions as part of their process streams rather than energy production. In the *Industrial Carbon Management Strategy*, published by EU, the need for carbon capture and storage (CCS) technologies for industry is highlighted (European Commission, 2024).

Gas separation processes based on adsorption are a well-established technology with solid sorbent CO₂ capture processes showing great potential due to their favourable LCA results (Petrescu et al., 2019). Adsorption based separation processes work through selective adsorption of molecules onto the surface of the sorbent under the release of adsorption energy. Sorbent regeneration occurs through either increase of temperature or reduction of the partial pressure and can be enhanced through utilization of a sweeping gas stream or purge. The general kinetics of the adsorption and desorption process are well researched for a large variety of sorbents, each presenting unique adsorption capacities (Helfferich and Ruthven, 1984; Yang, 1997).

Several classes of adsorbent materials are available for the capture of CO₂, including for example zeolites and metal-organic frameworks for low temperature applications, layered double hydroxides for intermediate temperatures (200-500 °C), and calcium-based adsorbents for high-temperature applications (>400 °C) (Wang et al., 2011). Importantly, layered double hydroxides or hydrotalcite-based adsorbents perform exceptionally well in terms of robustness, regenerability and capacity (Santamaría et al., 2023). As potassium-promoted hydrotalcite has been successfully scaled up for deployment in the sorption-enhanced water-gas shift (SEWGS) process (Sebastiani et al., 2022; Boon, 2023; Manzolini et al., 2020). All industrially relevant applications of CO2 adsorption are performed in the presence of steam - in general a complicating factor (Kolle et al., 2021). Potassium promoted hydrotalcite, however, is not only robust in the presence of steam (Coenen et al., 2017; Xin et al., 2024), it has been shown to interact with CO2 and steam which has allowed for the efficient use of steam as a working medium in CO₂ adsorption (Boon et al., 2014, 2015).

In this work, a comprehensive introduction to the novel technology DISPLACE, an isobaric adsorption process for CO₂ capture, is given. The separation is based on the promising behaviour of CO2 displacement by steam adsorption (Manzolini et al., 2022). Utilizing this unique characteristic of the sorbent, DISPLACE can be operated at an intermediate temperature and high pressure with high pressure products, the CO₂-lean and CO₂-rich streams. This technology has been validated on TRL 5 for the steelmaking industry as part of the Horizon 2020 project C⁴U (C4U website). In this project a proof-of-concept campaign was successfully performed on a single-column (3000 kg sorbent) pilot with a feed of 400 Nm³/h of exhaust gas from oxy-combustion BFG provided by the SSAB blast furnace in Lulea, Sweden. As this was a single-column campaign, the final cyclic performance was not demonstrated, but the potential for CO₂-rich product purities up to 99% and CO₂ capture rates of up to 95% for a multi-column operation was observed. Additionally, an intensive campaign on bench-scale for the validation of the process model and sorbent isotherms was performed. The results of both these campaigns are the basis for this paper which specifically describes the development of the technology in the context of decarbonising the steelmaking process.

The iron and steel industry poses significant challenges in reducing emissions. This industrial process accounts for approximately 7% of global direct energy-related CO2 emissions (International Energy Agency, 2020). This is primarily due to its heavy reliance on fossil fuels, particularly coal, in the blast furnace-basic oxygen furnace (BF-BOF) steelmaking route, which currently dominates the steel market with 70% production share (International Energy Agency, 2020). The integration of carbon capture technologies into steel production processes is crucial for advancing towards a net-zero emissions future. Perpiñán et al. (Perpiñán et al., 2023) performed a systematic review of peer-reviewed articles focusing on the integration of carbon capture technologies in the BF-BOF steelmaking route. The analysed carbon capture technologies were categorized into four main groups: i) post-combustion (chemical absorption (Manzolini et al., 2020; Gazzani et al., 2015; Yang et al., 2021), membranes (Yun et al., 2021; Luca and Petrescu, 2021; Baker et al., 2018)), ii) looping processes (calcium looping (Cormos et al., 2020; Tian et al., 2018; Xie et al., 2017), chemical looping (Luo et al., 2018; Katayama et al., 2020; Xiang and Zhao, 2018), other looping processes (Martínez et al., 2018; Sun et al., 2020)), iii) oxygen blast furnaces and top-gas recycling (Tsupari et al., 2015; Arasto et al., 2014; Li et al., 2020; Qie et al., 2020), iv) pre-combustion (chemical absorption (Gazzani et al., 2015; Chung et al., 2018a; Martinez Castilla et al., 2019), adsorption (Jin et al., 2017; Quader et al., 2016; Kim et al., 2015), membranes (Chung et al., 2018b; Jeon et al., 2022; Li et al., 2022; Ramírez-Santos et al., 2018), SEWGS (Petrescu et al., 2019; Manzolini et al., 2020; Gazzani et al., 2015; van Dijk et al., 2018)). The thermal penalty for various carbon capture technologies varies between 1.3 and 6.2 MJ/kg_{CO2}. Post-combustion chemical absorption (Chisalita et al., 2019; Biermann et al., 2019; Cormos, 2016), calcium looping (Tian et al., 2018), other looping processes (Fernández et al., 2017, 2020; Martínez et al., 2019), and pre-combustion chemical absorption (Chung et al., 2018b) exhibit different ranges within this spectrum. When it comes to electricity consumption, the differences are more pronounced. Post-combustion chemical absorption, calcium looping, and pre-combustion chemical absorption generally have lower electricity requirements, averaging less than 1 MJ/kg_{CO2}. This is because heat consumption is predominant, with most of electricity usage related to CO₂ compression. On the other hand, technologies like membranes (post- and pre-combustion), and adsorption pre-combustion requires a compression step upstream the CO2 capture process, leading to higher electricity penalties between 1 and 3 MJ/kg_{CO2}. From an economic perspective, post-combustion chemical absorption technologies demonstrate a linear relationship between CO₂ capture cost (€/t_{CO2}) and CO₂ emission reduction (kg_{CO2}/tsteel) ranging from 38 €/t_{CO2} for a CO₂ emission reduction of 400 kg_{CO2}/t_{steel} to 98 ℓ/t_{CO2} in the case of a reduction equal to 1700

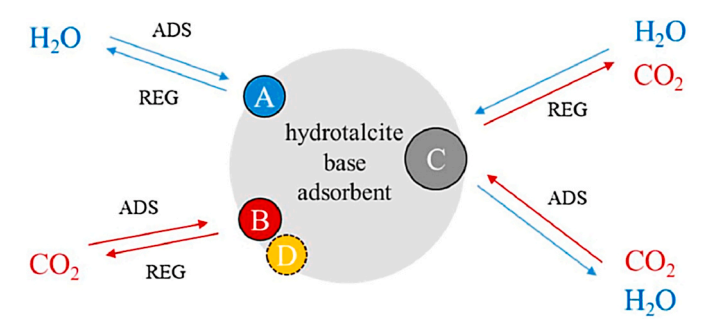


Fig. 1. Adsorption sites on the hydrotalcite based adsorbent for CO₂ and steam. Reprinted from (Coenen et al., 2018a).

kg_{CO2}/t_{steel} (Perpiñán et al., 2023). Conversely, oxy-blast furnace (Tsupari et al., 2015; Arasto et al., 2014) and calcium looping technologies (Cormos et al., 2020; Cormos, 2016) exhibit varying costs for equivalent levels of CO₂ emissions reduction. In the case of oxy-blast furnace, for a CO₂ reduction of 400 kg_{CO2}/t_{steel} the cost varies between 58 ϵ /t_{CO2} to above 90 ϵ /t_{CO2} (Perpiñán et al., 2023). In the instance of SEWGS technology, costs below 40 ϵ /t_{CO2} are achievable when the technology is employed for the gas fraction utilized as fuel within the steel mill's power plant (Manzolini et al., 2020).

Interestingly, Perpiñán et al. (Perpiñán et al., 2023) note a lack of literature on carbon capture applied to flue gas from oxy-combustion of steel-making gases (i.e. BFG, BOFG or COG). Therefore, this study aims to bridge this gap by introducing the innovative carbon capture technology named DISPLACE and its application to decarbonize the hot-stoves flue gas from oxy-combustion of blast furnace gas, which represents around 20% of the total CO₂ emissions of a BF-BOF plant. The integration of CCS technologies is recognised as fundamental in mitigating the carbon footprint of a BF-BOF steel mill (Perpiñán et al., 2023). Additionally, the results obtained enable the possibility of better understanding how to optimally run and integrate the DISPLACE technology in an industrial plant and to investigate its application to other CO₂ point sources within a steel mill.

The paper is organised as follows: in Section 2 the DISPLACE technology and the modelling approach are presented along with the methodology used to simulate the oxy-fired hot-stoves, the integration of DISPLACE in a steel plant and the principal KPIs; Section 3 presents and discusses the main results obtained, followed by the conclusion in Section 4.

2. Materials and methods

The simulation of the DISPLACE cycle process and its integration into the plant layout of a steel mill are detailed. The decarbonization of flue gas from hot-stoves serves as a specific case study.

An optimization process was conducted to determine the optimal

working temperature and pressure for DISPLACE. Elevating the pressure of the feed gas enhances CO_2 capture on the DISPLACE sorbent material, albeit at the cost of increased energy required for feed gas compression. Moreover, the consumption of regeneration steam, expressed as steam-to-carbon ratio, is a crucial parameter influenced by operating conditions. Higher temperatures result in a reduction of this ratio, offering favourable outcomes in terms of overall CO_2 emissions and cost efficiency.

The integration of the DISPLACE technology was executed using Aspen Plus V14, and the results were assessed via environmental Key Performance Indicators (KPIs). Furthermore, the performance of DISPLACE was compared against a conventional post-combustion amine-based carbon capture technology for comprehensive analysis.

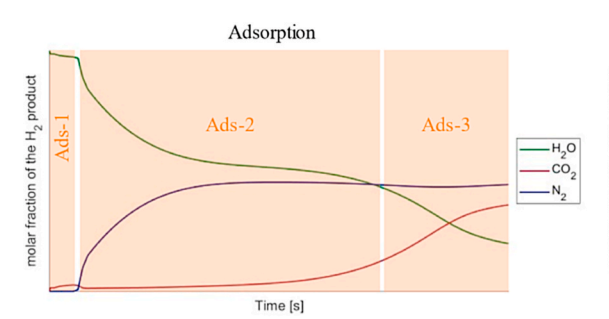
2.1. The DISPLACE technology

The DISPLACE technology is an isobaric separation technology for the post-combustion capture of CO2 from flue gases. It is based on a multicolumn concentration swing principle, which delivers the two separated product streams at the operating pressure of the unit. During the feed step, CO2 is adsorbed onto a sorbent leaving the stream CO2lean, while the sorbent is regenerated by displacing CO2 on the sorbent with steam leading to the CO2-rich product, without the need for a pressure or temperature swing. The basis of the process are the characteristic adsorption sites of the mixed base-metal oxide sorbent derived from hydrotalcites. This sorbent has several sites onto which CO2 and H₂O can adsorb (Fig. 1): site B and D are available for CO₂ adsorption and site C is a shared site. Detailed mechanical investigations have identified the presence of distinct sites for the interaction of CO₂ and steam with the adsorbent material (Coenen et al., 2018a). On shared site C, the adsorbed species (CO₂/H₂O) is the one with higher partial pressure in the gas phase. When the partial pressure ratio changes, the other species displaces the adsorbed species on the sorbent. The site can be assumed to only be occupied by one species at a time. The DISPLACE process utilises this displacement characteristics of site C to achieve high purity CO2 product at high capture ratios.

2.1.1. DISPLACE cycle development

The product of a single column separation process without recycles and using gases from BFG oxy-combustion is shown in Fig. 2 (nitrogen is present in BFG and not introduced with the oxidant). The process consists of two steps: adsorption and desorption, both of which can be divided into three sections: 1) void composition, 2) pure product, 3) product tail.

In the case of the adsorption step, the first section (Ads-1) is comprised of a steam-CO₂ mixture which remained in the void fraction after the preceding regeneration (Des-3). The second section is the CO₂-lean product (Ads-2), which in this case is mostly nitrogen coming with the BFG. The third section is the product once the CO₂ breaks through (Ads-3). Equally, for the desorption step, the first section (Des-1) is the



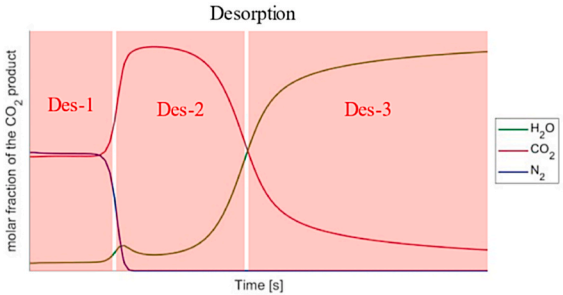


Fig. 2. Product compositions (wet) of a single column DISPLACE process operated at 15 bar and 400 $^{\circ}$ C without recycles: adsorption (left) and desorption (right). The column was modelled at 2 m height, 0.038 m diameter with a feed flowrate of 15 slpm (2.3% $_{2}$ H₂O, 48% $_{2}$ CO₂, 49.7% $_{2}$ N₂) and a counter current steam flow of 12 slpm (100% $_{2}$ H₂O).

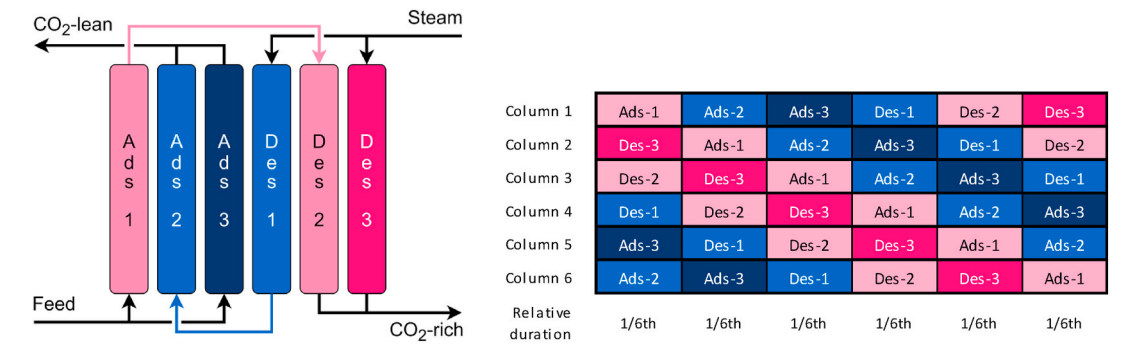


Fig. 3. Six column DISPLACE process for a CO₂-N₂ separation (left) and timing for a 6-column unit (right). The column names indicate which product gas they are producing.

Table 1
Mass transfer equations of the 1D heterogeneous column taken from (Boon et al., 2014).

Continuity	$\frac{\partial \rho}{\partial t} = -\frac{\partial \rho v}{\partial z} + \frac{1 - \epsilon_b}{\epsilon_b} a_p \sum_i M_i N_i$	(1)
Momentum	$0 = -\frac{\partial \mathbf{p}}{\partial \mathbf{z}} - f \frac{\rho u u}{d_p}$	(2)
Mass balance	$rac{\partial (ho \omega_i)}{\partial t} = - rac{\partial ho v \omega_i}{\partial z} + rac{\partial}{\partial z} igg(D_z ho rac{\partial \omega_i}{\partial z} igg) + $	(3)
*	$\frac{1-\epsilon_b}{\epsilon_b}a_pM_iN_i$	(1)
Intraparticle mass balance	$rac{\partial \langle c_i angle}{\partial { m t}} = k_{LDF,i} ig(c_{int,i} - \langle c_i angle ig)$	(4)

remaining feed composition in the void volume of the column. The second section is a high purity and very dry CO_2 stream (Des-2). In the third section still more CO_2 is desorbed, while steam is breaking through (Des-3).

The basic design constraints for the cycle development of the continuous process are.

- one column needs to always receive feed;
- one column needs to always produce CO2-lean product;
- one column needs to always produce CO2-rich product;
- reduction of the steam consumption by recycling Ads-1 within the cycle;
- increase of the CO₂ purity by recycling Des-1 within the cycle.

These constraints lead to the adoption of at least six columns. Furthermore, to avoid build-up of impurities in the system, there should always be a "flush" after a column received a recycled stream which means that the following step should feed more gas than just replacing the void volume. Taking all the constraints and the process considerations into account while minimizing the number of columns, the six column set-up is identified as the optimal configuration and represented in Fig. 3 together with the corresponding timing.

As the product of Ads-1 is mostly steam with some CO_2 , it is recycled to the desorption step (Des-2) to reduce the steam demand of the process. Any potential impurity build-up in the desorption step due to this recycle is avoided by following the recycle feed with regeneration steam. Likewise, the product from Des-1 which is a similar to feed composition is recycled to the adsorption step to increase the CO_2 -product purity. Any impurities from this recycled stream are flushed out of the system through feed gas in Ads-3.

The adsorption is performed co-currently while desorption is performed counter-currently to keep the end of the bed as clean as possible improving the product purity. A clean sorbent can adsorb ${\rm CO_2}$ at very low partial pressures preventing slip.

Alternative processes involving more columns or more complex

mixed recycles are possible and would allow for further optimization. However, this simple set-up fulfils the basic need of the process and allows for the best understanding of the characteristics.

2.1.2. DISPLACE modelling

DISPLACE uses an existing model which contains experimentally validated correlations for the interaction, the mass-transfer and the 1D heterogeneous column models (Boon et al., 2014; Coenen et al., 2018b; Sebastiani et al., 2021). The basic equations used within the model are the continuity, momentum and mass balance for a column filled with a sorption bed as well as the specific equation for the intra particle mass transfer using the linear driving force approximation (Table 1).

As the DISPLACE process is operated isobarically with recycles, the column model was built to include and account for column pressure drops for the recycles. The interaction and mass-transfer models have previously been experimentally validated for low to high CO $_2$ and H $_2$ O concentrations (0–100%), in a temperature range of 350 °C–450 °C and adsorption and desorption pressure between 10 - 25 bar and 1–4 bar, respectively (Sebastiani et al., 2021). DISPLACE operation is at or just outside these boundaries concerning: i) the operation at temperatures as low as 300 °C and ii) CO $_2$ desorption with 100% H $_2$ O at increased pressure as high as 15 bar. The interaction model needed finetuning for both these aspects and experimental results were used for renewed model validation. This will be presented in a future work.

2.1.3. DISPLACE cycle optimization

Optimizing the DISPLACE process for a specific process integration is a multivariable process. The most impactful parameters are: (i) system pressure, (ii) column size (diameter and height), (iii) number of trains, (iv) cycle step lengths and (v) steam-to-carbon (S/C) ratio of the desorption steam feed relative to the flue gas adsorption feed. Specific performance in terms of $\rm CO_2$ -purity at dry conditions (CP, equation (5)) and carbon capture ratio (CCR, equation (6)) are defined by the process integration and downstream unit requirements (Section 2.2). As a result of the column size, the cycle time and the captured $\rm CO_2$, a process productivity is derived. The productivity (equation (7)) is a measure on how effectively the sorbent material has been used. A higher productivity indicates less sorbent needed for the same amount of $\rm CO_2$ captured. A sensitivity study on the process parameters is conducted where above-mentioned parameters are varied to identify the most suitable performance.

$$CP[\%] = \frac{(\dot{n}_{CO_2})_{CO_2-product,dry}}{\sum_{i} (\dot{n}_i)_{CO_2-product,dry}} \cdot 100 \tag{5}$$

$$CCR[\%] = \frac{(\dot{m}_{CO_2})_{CO_2 - product}}{(\dot{m}_{CO_2})_{feed}} \cdot 100$$
 (6)

Table 2Oxy-fired hot-stoves streams with corresponding thermodynamic conditions.

Stream	m	T	P	Compos	Composition [%vol]						
	[kg/s]	[°C]	[bar]	H ₂	CO ₂	СО	O ₂	N ₂	Ar	H ₂ O	
Ambient air [1]	135.43	12	1.013	_	0.04	_	20.72	77.22	0.92	1.10	
Oxygen [2]	7.26	60	1.1	_	-	_	99.9	0.01	0.09	_	
Steam [3]	0.84	175	9	_	-	_	_	_	-	100.0	
Hot blast air [4]	144.09	1118	4	_	0. 04	_	24.13	72.98	0.87	1.98	
BFG [5]	77.21	30	1.11	2.3	20.54	21.79	_	51.36	_	4.01	
O ₂ for combustion [6]	10.66	60	11	_	_	_	99.9	0.01	0.09	_	
Hot-stoves flue gas [7]	87.88	140	1.01	-	41.90	-	1.00	50.81	0.04	6.25	

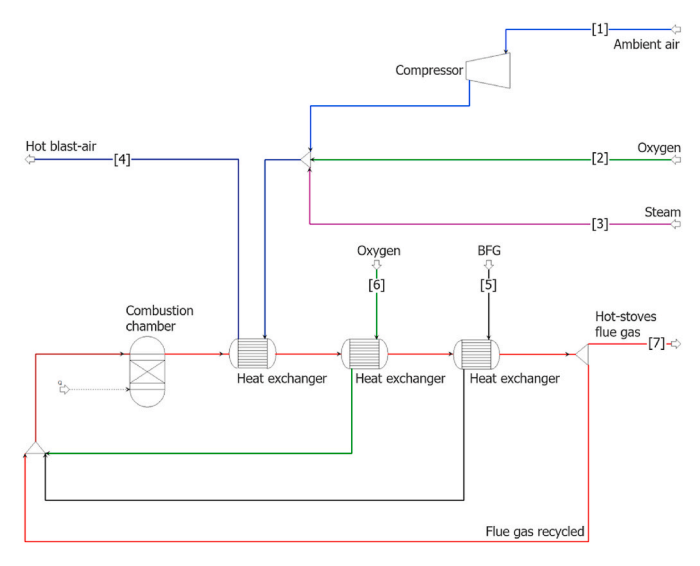


Fig. 4. Aspen Plus simulation of oxy-fired hot-stoves.

Productivity
$$\left[\frac{\text{mol}_{\text{CO}_2}}{\text{kg}_{\text{sorbent}}h}\right] = \frac{(\dot{n}_{\text{CO}_2})_{\text{CO}_2-\text{product}}}{m_{\text{sorbent}}}$$
 (7)

2.2. DISPLACE technology applied to gas from a steel plant

The integration of the DISPLACE technology into a blast furnace-basic oxygen furnace steel mill has been examined. In this section, the innovative decarbonization process applied to the hot-stoves flue gases is presented. Since this is the first time that the DISPLACE process is evaluated, several operating temperatures and pressure were explored to identify the optimal region.

2.2.1. Flue gas from the hot-stoves

In a conventional steel mill, the reduction of iron-bearing materials, such as iron ore lump, sinter and/or pellets, takes place in the blast furnace. These materials, along with additives (i.e. limestone) and reducing agents (i.e. coke) are fed from the top of the furnace. Additionally, hot blast air, enriched with oxygen, is injected in the lower part of the furnace guaranteeing the production of carbon monoxide from coke and therefore, the reduction of iron ores into metallic iron (Remus et al., 2013).

The hot-stoves are high-temperature heat exchangers in which cold ambient air is heated up to the desired temperature (900–1350 $^{\circ}$ C). They are operated on a cyclical basis. A mix of BFG and COG is usually used as fuel to generate hot combustion gases that are circulated through a network of pipes and chambers made of heat-resistant refractory materials until these materials reach the correct temperature (1100–1500 $^{\circ}$ C). Then the combustion gases are cut off and the cold ambient air is introduced in the opposite direction. The hot bricks release the heat to the cold air in contact with them. The cycle lasts until the blast air can reach the desired temperature. Subsequently a new

cycle is started (Remus et al., 2013).

Within the C^4U project, the adoption of oxy-fired hot-stoves has been proposed. In this case, only BFG is used as fuel, and it is burnt with oxygen instead of air. This has the double effect of lowering the amount of BFG used in the hot-stoves and increasing the concentration of CO_2 in the flue gases effectively favouring the carbon capture process. It must be pointed out that the CO_2 will still be diluted in the exhaust gases as BFG contains relevant amount of N_2 (around 51% as reported in Table 2).

The optimal incorporation of the DISPLACE technology into the steel mill layout has been carried out considering diverse operating conditions in terms of temperature and pressure. The focus has been specifically on cases where carbon capture exceeds 90%, ensuring a minimum carbon purity of 95% on dry basis. Through comprehensive simulations of the DISPLACE cycles, key parameters, including the number of columns, size dimensions, and steam consumption, have been accurately computed.

To assess the integration of DISPLACE technology, Aspen Plus V14 has been employed, utilizing the cycle performances determined in the preceding step.

2.2.2. Thermodynamic assessment – hot-stoves simulation

The oxy-fired hot stove have been simulated in Aspen Plus V14 using the RKS-BM property model (Fig. 4). The mass flow rate of cold air, oxygen and steam has been adapted from (IEAGHG Technical Report, 2013) considering the same specific mass flow (kg/t_{HRC}) and the same thermodynamic conditions. Therefore, the composition, temperature and pressure of hot blast air are the same as reported in (IEAGHG Technical Report, 2013). The Aspen Plus model thus has been used to compute the mass flow rates of the BFG and the oxygen used for combustion as well as the composition of the flue gas.

In this study a conventional steel mill producing 3.16 Mt_{HRC}/y is considered. The mass flow rate of BFG used as fuel in the hot-stoves is equal to 77.21 kg/s corresponding to 1.60 GJ/t_{HRC}. The CO₂ emissions associated to the hot-stoves flue gas are 47.47 kg_{CO2}/s equal to 0.443 t_{CO2}/t_{HRC}. The resulting gas conditions are shown in Table 2 and refer to the streams of Fig. 4.

2.2.3. Thermodynamic assessment - DISPLACE integration

The plant scheme of the integration of the DISPLACE technology for decarbonization of flue gas from hot-stoves is shown in Fig. 5. The flue gas from hot-stoves (red stream) is at 140 °C and slightly above the atmospheric pressure. Before being compressed, it is cooled to 35 °C to minimize compression work and contributing to the pre-heating up to 102 °C of a portion of the water used for generating steam, utilized in the DISPLACE columns. Similarly, the outlet gas streams from the DISPLACE process, i.e. the CO₂-rich stream (grey stream) and the CO₂-lean gas stream (green stream), are cooled generating steam. A furnace is adopted to supply the heat to the gas stream exiting the compressor and for superheating of the steam to the DISPLACE working temperature. This furnace alternately uses NG and COG as fuels. Prior to entering the furnace, the fuel and combustion air are preheated by the furnace flue gases (black stream). To prevent the presence of non-condensable

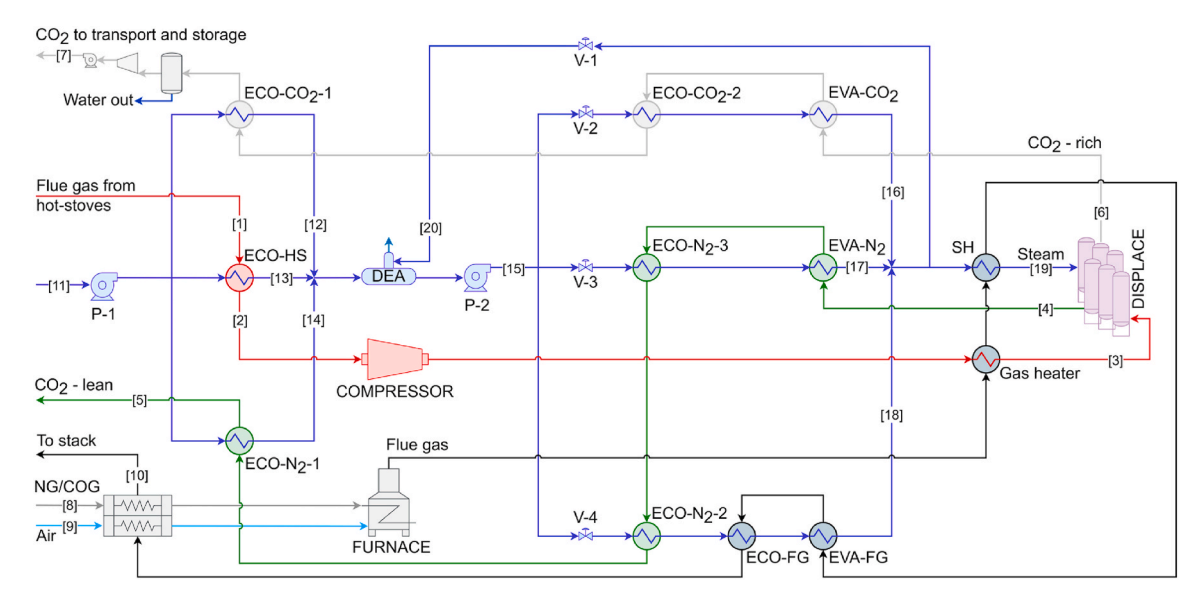


Fig. 5. Plant scheme of the integration of DISPLACE technology for decarbonization of flue gas from hot-stoves.

 Table 3

 Assumptions for the thermodynamic assessment.

Parameter	Unit	Value
NG LHV	MJ/kg	46.87
COG LHV	MJ/kg	40.21
Electricity CO ₂ emissions	kg _{CO2} /MWh	250
Water recovery from CO2 stream	%	90
Plant availability	h/y	8200
Steel plant capacity	Mt_{HRC}/y	3.16
Heat Exchangers		
- Minimum ΔT gas-gas heat exchanger	°C	15
- Minimum ΔT gas-liquid heat exchanger	°C	10
- ΔT subcooling in the economizers	°C	5
- Economizer hot-side pressure drops	bar	0.2
- Economizer cold-side pressure drops	bar	0.7
- Evaporator hot-side pressure drops	bar	0.2
Turbomachines		
- Pumps hydraulic efficiency	%	75
- Pumps mechanical efficiency	%	95
- Compressor polytropic efficiency	%	85
- Compressor mechanical efficiency	%	95
${\rm CO_2}$ compression train		
- Compressor number of stages	-	3
- Compressor discharge pressure	bar	80
- Compressor polytropic efficiency stage 1,2	%	80
- Compressor polytropic efficiency stage 3	%	75
- Compressor mechanical efficiency	%	95
- Pump discharge pressure	bar	110
- Pump hydraulic efficiency	%	75
- Pump mechanical efficiency	%	95

Table 4Assumptions adopted in the Aspen model of the MEA carbon capture sections.

	•	
Unit	Aspen Plu	s model
Absorber	RadFraq	Rate-Based; 25 stages; MELLAPAK 250Y; Condenser: None; Reboiler: None
Stripper	RadFraq	Rate-Based; 20 stages; MELLAPAK 250Y; Condenser: Partial-Vapor-Liquid; Reboiler: Kettle
Heat exchanger	HeatX	Pinch point $\Delta T = 10$ °C
Pump	Pump	Discharge pressure = 2.5 bar; $\eta_h = 0.75$; $\eta_m = 0.95$
CO_2	Mcompr	3 stages; Discharge pressure = 80 bar; $\eta_{p,1,2} = 0.8$; $\eta_{p,3}$
compression		= 0.75; η_m = 0.95; $T_{\rm intercooling}$ = 28 °C
	Pump	Discharge pressure = 110 bar; $\eta_h = 0.75$; $\eta_m = 0.95$

Table 5Assumptions for the economic assessment.

Parameter	Unit	Value
NG/COG price	€/MWh	50
Electricity price	€/MWh	125
Discount rate	%	8.00
Lifetime	years	25
Fixed Charge Factor	%	9.37
Water cost	€/m ³	1
N° additional employees per CC section	_	15
Annual salary	€/y	60000
O&M costs	% TPC•FCF	5

species in the steam, a deaerator was included (Fig. 5). The $\rm CO_2$ -rich stream is taken to the conditions for transport and storage (110 bar) through a multistage compressor, reaching pressures of up to 78 bar, liquefaction to 25 °C and subsequently pumped to a pressure of 110 bar as described in (Wright et al., 2011; Zecca et al., 2023). The specifications of the streams indicated in Fig. 5 are given in Appendix 5.1. Since many different operating conditions of DISPLACE were analysed in this work, as detailed in the following chapters, only the results regarding the case 5 bar–400 °C are shown.

Simulations of DISPLACE integration were performed using Aspen Plus 14, incorporating the assumptions detailed in Table 3. The composition of natural gas (NG) and coke oven gas (COG) were taken from (IEAGHG Technical Report, 2013).

${\it 2.2.4.} \ \ {\it Reference technology-MEA post-combustion carbon capture}$

The reference technology adopted in this study to assess DISPLACE performance is the widely used post-combustion technology based on MEA scrubbing. According to the authors' knowledge there is no commercially available large scale $\rm CO_2$ capture system based on physical adsorption, therefore MEA which is a well proven and commercially ready technology was selected for comparison.

A detailed description of the process can be found in (Zecca et al., 2023). The MEA post-combustion $\rm CO_2$ capture process has been simulated in Aspen Plus V14 using the unsymmetric electrolyte NRTL property method (ENRTL-RK). The model includes the following key features: (i) true species including ions, (ii) activity-based reaction kinetics, (iii) rate-based models for columns with structured packing.

The electrolyte solution chemistry has been modelled with a CHEMISTRY model as the global electrolyte calculation option in the simulation. Chemical equilibrium is assumed with all the ionic

Table 6 PEC of electricity generation.

Parameter	Unit	RES	NGCC	USC
Electricity C.I. Plant efficiency	[kg _{CO2} /MWh _e] [MW _e /MW _{LHV}]	0 -	350 0.60	850 0.42
PEC electricity generation	$[MWh_{LHV}/MWh_{e}]$	0	1.67	2.38

reactions. In addition, a REACTION model has been created and used to model the reactions occurring in the absorber and in the stripper. All reactions are assumed to be in chemical equilibrium except those of $\rm CO_2$ with $\rm OH^-$ and $\rm CO_2$ with MEA. The assumptions used to model the carbon capture section in Aspen Plus are shown in Table 4 while more details are provided in section5.2.

2.2.5. Economic assessment

In this section, the methodology adopted to perform the economic assessment is described. General assumptions are summarized in Table 5. The electricity and NG prices were computed using the data reported in (International industrial energy prices). For both of them, average values in EU have been calculated considering the prices of 2019 and 2022. In the case of electricity, annual industrial electricity prices including environmental taxes and levies for very large consumers were considered. Similarly, for NG, annual industrial prices including taxes for large consumers were used. The price of COG is assumed to be the same of NG on energy basis.

The total plant cost (TPC) was computed starting from equipment costs according to the bottom-up methodology described in (Manzolini et al., 2020).

Focusing on the DISPLACE technology, the TEC is calculated using equations (8)–(11).

$$TEC_{DISPLACE}[\ell] = c_{columns} + c_{bulk \ material \ and \ freight} + c_{valves}$$
(8)

$$c_{valves}[\boldsymbol{\epsilon}] = \sum_{i=i}^{n} \left(c_{valve,i} \cdot n_{valves \; per \; column,i} \cdot n_{colums \; per \; train} \cdot n_{train} \right) \tag{9}$$

$$c_{columns}[\ell] = c_{steel}[\ell/kg] \cdot m_{column} \cdot n_{colums per train} \cdot n_{train}$$
 (10)

$$c_{\text{bulk material and freight}}[\ell] = 0.77 \cdot c_{\text{columns}}$$
 (11)

The DISPLACE total plant cost (TPC) is calculated from TEC using equations (12) and (13) and the values shown in Table 13.

$$TDC_{DISPLACE}[\ell] = TEC_{DISPLACE} + c_{construction} + c_{other}$$
(12)

$$TPC_{DISPLACE}[\ell] = TDC_{DISPLACE} + EPCM_{services} + c_{contingency}$$
 (13)

The total plant cost (TPC) of the auxiliary equipment (i.e. compressors, furnaces, heat exchangers, etc.) and of the MEA carbon capture section were computed through equations (35)–(39) and using the values reported in Table 14.

Finally, the total annualised cost (TAC) is computed considering: i) the total plant cost (TPC) annualised through the fixed charge factor (FCF); ii) the variable costs as the cost of electricity (C_{el}), the cost of natural gas (C_{NG}), the cost of water (C_{H_2O}); iii) the fixed costs (C_f); and iv) the operation and maintenance costs ($C_{O\&M}$).

$$TAC\left[\frac{M \varepsilon}{y}\right] = TPC \cdot FCF + C_{el} + C_{NG} + C_{H_2O} + C_f + C_{0\&M} \tag{14} \label{eq:14}$$

More details on the procedure adopted to perform the economic assessment of the MEA and DISPLACE technologies are given in the appendix (section 5.4).

2.3. Key performance indicators

The evaluation of the performance of the DISPLACE carbon capture technology is made through environmental and economic key perfor-

mance indicators, typical of this research field and available in (Manzolini et al., 2020; Zecca et al., 2023; Khallaghi et al., 2022). The environmental indexes considered in this study are the primary energy consumption (PEC), the specific CO_2 emissions (e_{CO_2}), the CO_2 capture ratio (CCR), the specific primary energy consumption for CO_2 avoided (SPECCA) and CO_2 avoidance (CA). The SPECCA indicator is defined as the additional primary energy required (in GJ) to avoid the emission of 1 ton of CO_2 producing the same amount of product.

$$PEC\left[\frac{GJ_{LHV}}{t_{HRC}}\right] = \frac{\dot{m}_{fuel}LHV_{fuel} + PEC_{el} + \dot{Q}_{req}/\eta_{th}}{\dot{m}_{HRC}}$$
(15)

$$e_{\text{CO}_2} \left[\frac{t_{\text{CO}_2}}{t_{\text{HRC}}} \right] = \frac{\dot{m}_{\text{CO}_2}}{\dot{m}_{\text{HRC}}} \tag{16}$$

$$SPECCA \left[\frac{GJ_{LHV}}{t_{CO_2}} \right] = \frac{PEC_{capture} - PEC_{no\ capture}}{e_{CO_2,no\ capture} - e_{CO_2,capture}}$$
 (17)

$$CA[\%] = \frac{e_{CO_2,no \text{ capture}} - e_{CO_2,capture}}{e_{CO_2,no \text{ capture}}} \cdot 100$$
(18)

The PEC associated to the electricity generation varies in relation to its carbon footprint. In this study, the values provided in Table 6 are taken as reference and linear interpolation is employed for intermediate scenarios. In the renewable energy scenario, where the carbon intensity of imported electricity from the grid is 0 kgCO2/MWhe, implying no fossil fuel consumption during operation, hence ignoring the carbon footprint of green electricity production, the PEC related to electricity generation is deemed as 0 MWhLHV/MWhe. When the electricity carbon intensity reaches 350 kgCO2/MWhe, it is assumed that the electricity is generated in a natural gas combined cycle (NGCC) plant with an efficiency of 60%. Another scenario considered involves a coal ultra-supercritical cycle (USC), having an efficiency of 42% and a carbon footprint of 850 kgCO2/MWhe.

The economic performance is assessed in terms of levelized cost of hot rolled coil (LCOHRC) and cost of CO_2 avoidance (CCA). In equation (19), τ indicates the plant availability.

$$LCOHRC\left[\frac{\varepsilon}{t_{HRC}}\right] = \frac{TAC}{\dot{m}_{HRC} \cdot 8760 \cdot \tau} \cdot 10^{6} \tag{19}$$

$$CCA \left[\frac{\epsilon}{t_{CO_2}} \right] = \frac{LCOHRC_{capture} - LCOHRC_{no \ capture}}{e_{CO_2, no \ capture} - e_{CO_2, capture}}$$
 (20)

3. Results and evaluation

3.1. DISPLACE performance at different operating conditions

The DISPLACE performance is modelled using hot-stoves off gases as reported in Table 2 and assuming operating temperatures ranging from 300 °C to 400 °C. The process comprises four trains, each consisting of six columns. The height of each column is fixed at 16 m, with varying diameters: 3, 3, 2.75, and 2.5 m, corresponding to operating pressures of 5, 6, 7, and 10 bar, respectively. The diameter is mainly influenced by the volumetric flowrate and allowable linear gas velocity as well as the amount of sorbent required (based on the working capacity). Generally, in adsorption based separation systems a high system pressure and thus a high partial pressure of the adsorbing components leads to an increase of the sorbent capacity. However, for DISPLACE most of the capacity results from the displacement site, on which the adsorption of CO2 and steam are independent of system pressure. High gas velocity creates an adsorption process limited by the mass transfer to the sorbent (equation (4)) while a low velocity leads to a process driven by axial dispersion rather than convection. The optimal velocity lies in between, leading to a sharp mass transfer zone resulting in high purity products and the best utilization of the adsorbent in the column. A higher utilization leads to a higher productivity as defined in equation (7). In order to model the

Table 7Linear driving force parameter [s⁻¹] range for each step of the DISPLACE process.

Pressure	Parameter	Ads-1	Ads-2	Ads-3	Des-1	Des-2	Des-3
5 bar	CO_2 k_{LDF}	0.02-0.22	0.02-0.20	0.02-0.22	0.02-0.27	0.03-0.3	0.03-0.22
	H_2O k_{LDF}	0.04-0.35	0.04-0.25	0.02 - 0.16	0.02-0.35	0.05-0.35	0.1 - 0.35
10 bar	CO_2 k_{LDF}	0.02-0.8	0.05-0.4	0.1-0.36	0.03-0.7	0.05-0.75	0.03-0.7
	H_2O k_{LDF}	0.02-0.2	0.02 – 0.18	0.02 – 0.15	0.02 – 0.2	0.02 – 0.2	0.02 – 0.18

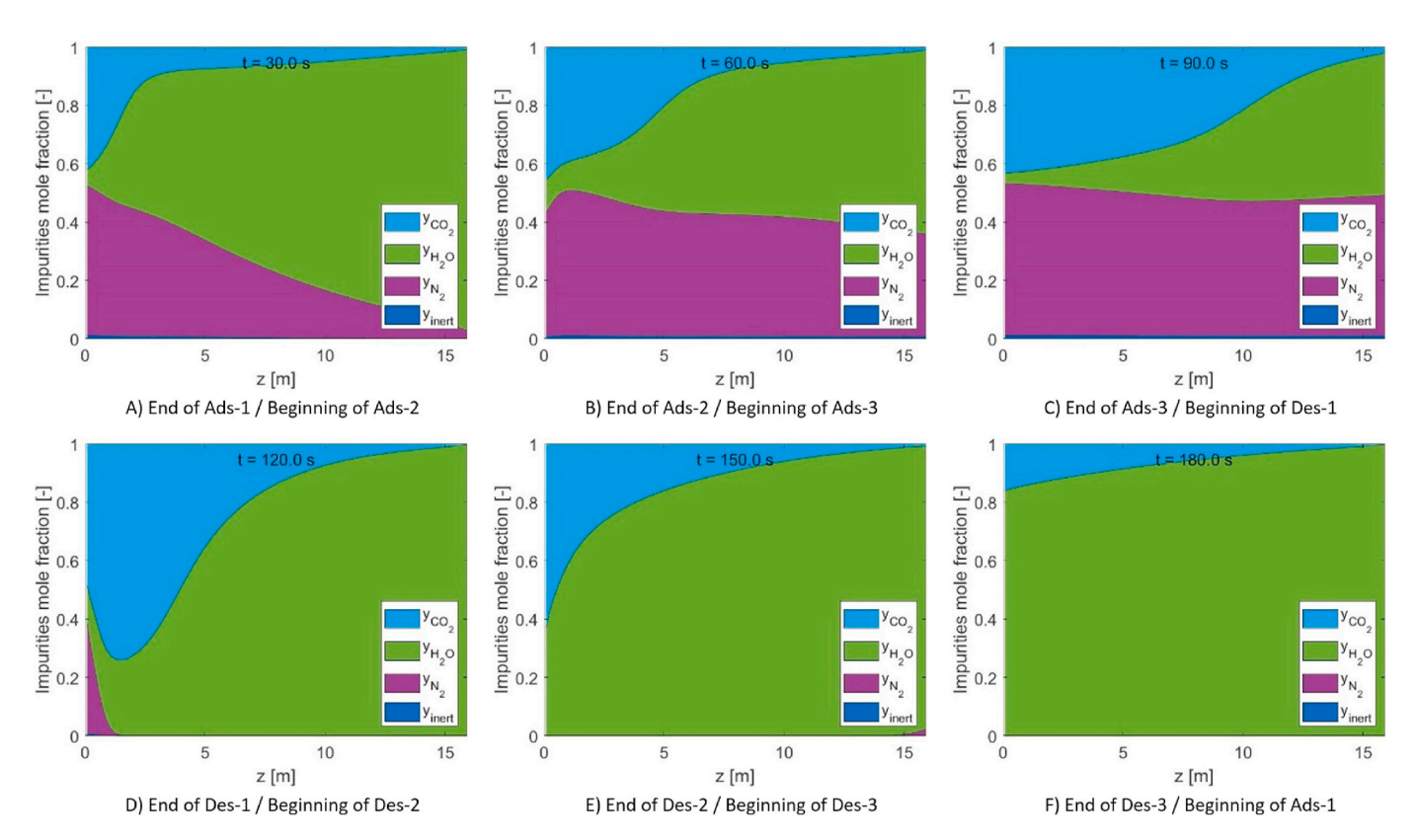


Fig. 6. Composition of the gas phase in the void fraction of the column for each step for a cycle operated at 10 bar with a CCR of 99.4% and a CP of 98.6%. The top three steps are after being fed co-currently (left-to-right) the bottom three steps are after being fed counter currently (right-to-left).

mass transfer from the bulk gas phase and the adsorption site, a linearised correlation for intraparticle resistance to mass transfer is introduced. Characteristic values for the linear driving force to the sorbent,

 k_{LDF} , are listed for each step in Table 7. These values are a function of intraparticle diffusion, sorbent pellet diameter and slope of the isotherm. Due to the Langmuir-like shape of the isotherm, the slope of

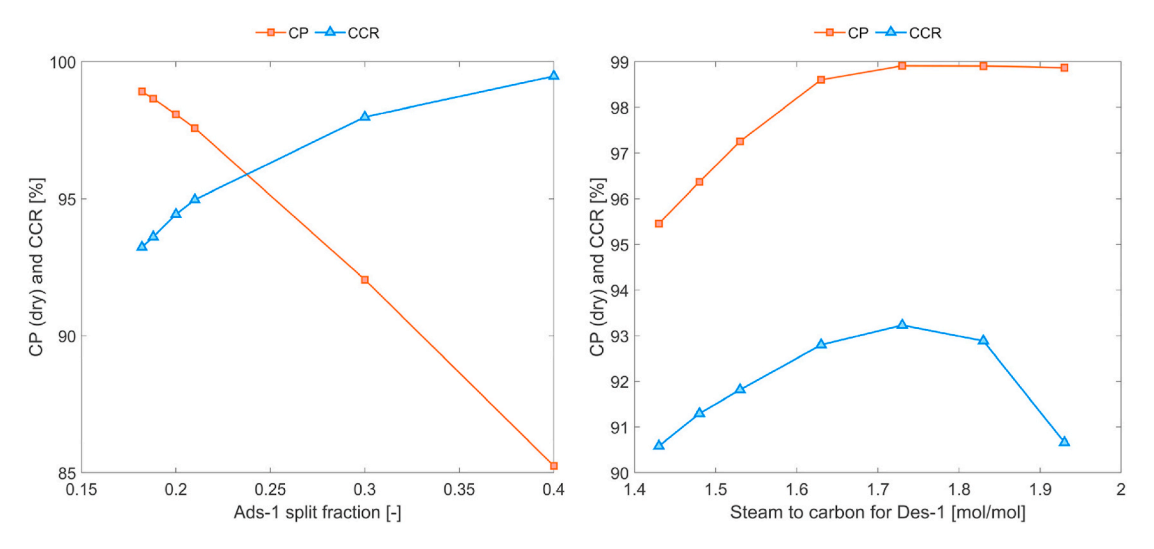


Fig. 7. Behaviour of the system at 6 bar and 400 °C for different feed split ratio for Ads-1/Ads-3 (left) and different S/C ratios fed to the first desorption step (right) while keeping all other design parameters constant.

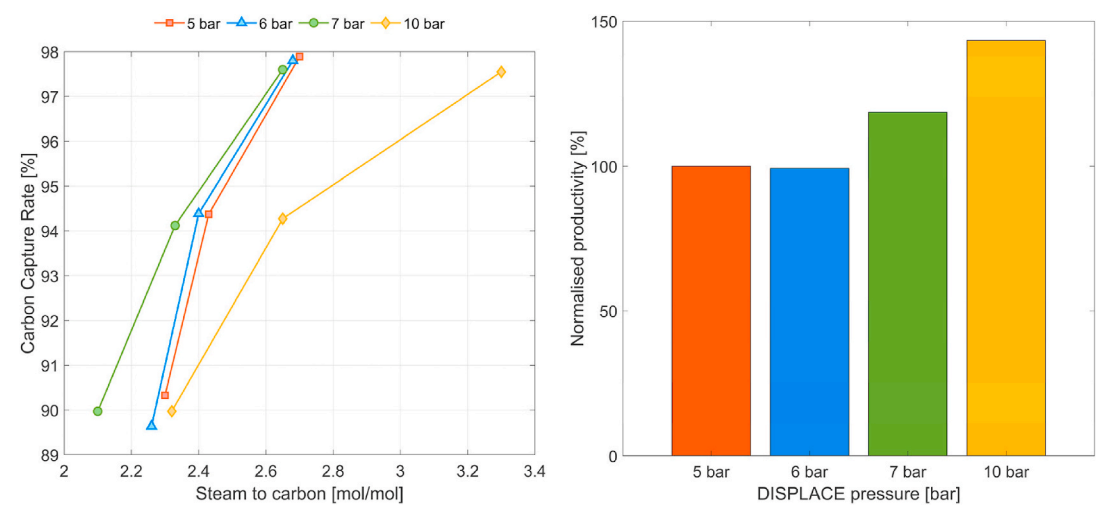


Fig. 8. Trade-off between steam demand and carbon capture rate (left) and between system pressure and productivity (right) with the productivity normalised to the 5 bar case. Unless otherwise stated the CCR is 90%, the CP 95% and the temperature is 400 °C.

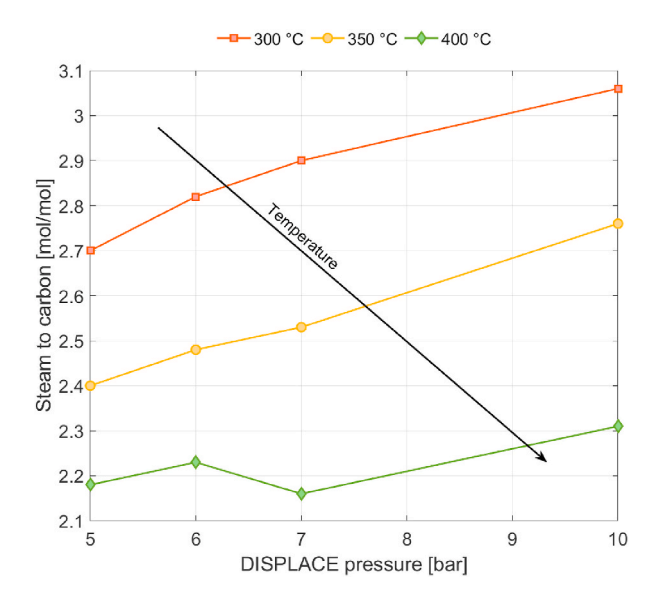


Fig. 9. Steam-to-carbon as function of DISPLACE working temperatures and pressures (CCR = 90%, CP = 95%).

the isotherm is very steep for low partial pressures leading to low k_{LDF} values which in turn results in lower mass transfer towards the sorbent.

Fig. 6 shows an example of the gas composition of the void fraction gas phase in the column after each step. This in turn means it is the starting composition for the following step.

- At the end of Ads-1, the column has been fed with feed gas to the point that a small amount of N₂ has broken through. The outlet of this column is fed to Des-2 where we can see this N₂ in the gas phase of the column.
- Ads-2 has been fed with the gas of the void volume from Des-2 which
 is what is left in the column after the adsorption step. This recycle
 stream is similar in composition to the feed stream.
- Finally in Ads-3 the column is fed with feed gas until a specific amount of CO₂ breaks through.
- The near-feed composition in the column is then flushed out with steam in Des-1 and recycled to Ads-2. The remainder of the column shows the block plug of CO₂ which has been formed by displacing CO₂ from the sorbent with steam.

- The column state at the end of Des-2 is the result from recycling the steam from Ads-1 with a small amount of N₂ breakthrough
- In Des-3 the column is fully flushed with steam to achieve a high degree of regeneration.

The results from the parametric analysis show a high dependency of the process performance on the flowrates towards Ads-1 and Des-1. As these steps determine the amount and composition of the recycled gas, they directly influence the purity of the CO_2 product and the preloading of the sorbent. If Ads-1 is fed too much or Des-1 is fed too little, then large amount of impurities go towards the CO_2 product, thus reducing the CO_2 purity (Fig. 7, left). Additionally, if Des-1 is fed with too much steam, then the CO_2 plug is recycled to Ads-2 and will occupy adsorption sites effectively reducing the working capacity of the system, leading to a reduced CCR (Fig. 7, right).

Next to the flowrates to Ads-1 and Des-1 the temperature of the system impacts the working capacity of both steam and CO_2 , as shown in Fig. 9. At lower temperature, the capacity to adsorb CO_2 increases, reducing the amount of required sorbent. However, the capacity to adsorb steam increases even further leading to larger steam demands per mol of CO_2 fed. So, while the system is operated at a lower temperature and thus will require less heating of the feed stream, the steam demand increases.

Overall, the sensitivity studies show a trade-off between CCR and CP vs. steam demand (Fig. 7, right), productivity vs. system pressure (Fig. 8) and steam demand vs. temperature (Fig. 9), thus allowing several operating points and system designs to achieve the same performance. In Fig. 8, cases at 400 $^{\circ}$ C with a carbon purity of 95% and, unless otherwise mentioned, a carbon capture ratio of 90% are shown. The figures clearly show the thermodynamic advantage of DISPLACE to operate at pressure below 7 bar, but from an economic point of view, the higher the pressure the higher the productivity is with advantages on the process costs.

In Table 8, the molar flow rate as well as the composition of the CO₂-rich stream leaving the DISPLACE column is indicated. As can be observed in Fig. 9, increasing the working temperature has the beneficial effect of diminishing the steam-to-carbon ratio.

After analysing the simulations corresponding to the cases outlined in Table 8, as depicted in Figs. 10 and 13, it was observed that the best results were achieved at 400 °C. This confirms the advantageous impact of elevating the operating temperature of DISPLACE, which in turn diminishes the steam-to-carbon ratio, thereby reducing the amount of steam required for CO_2 capture, as illustrated in Fig. 9. Consequently, additional simulations were conducted at 400 °C, exploring various values of carbon purity (CP) – 95%, 97%, and 99% – and carbon capture

Table 8 DISPLACE performance at different operating conditions with corresponding CO_2 rich stream thermodynamic conditions.

Case	Unit	1	2	3	4	5	6	7	8	9	10	11	12
P	bar	5	5	5	6	6	6	7	7	7	10	10	10
T	°C	300	350	400	300	350	400	300	350	400	300	350	400
D	m	3	3	3	3	3	3	2.75	2.75	2.75	2.5	2.5	2.5
CP	%	95.41	95.27	95.41	95.26	95.22	95.45	95.22	95.24	95.64	95.16	95.30	95.32
CCR	%	91.20	90.71	90.38	90.20	90.25	90.58	90.27	90.11	90.85	90.12	90.05	90.19
S/C	mol/mol	2.70	2.40	2.18	2.82	2.48	2.26	2.90	2.53	2.16	3.06	2.76	2.31
CO2 stream	kmol/s	1.56	1.45	1.38	1.38	1.32	1.28	1.62	1.48	1.32	1.51	1.50	1.36
CO ₂ -rich stream	n composition a	t reactor out	let										
- Ar	%vol	0.06	0.07	0.07	0.07	0.07	0.07	0.06	0.06	0.07	0.06	0.06	0.07
- Ar - H ₂ O	%vol %vol	0.06 33.89	0.07 29.15	0.07 26.00	0.07 26.07	0.07 22.28	0.07 20.09	0.06 36.85	0.06 30.81	0.07 22.25	0.06 32.26	0.06 31.93	0.07 24.73
- H ₂ O	%vol	33.89	29.15	26.00	26.07	22.28	20.09	36.85	30.81	22.25	32.26	31.93	24.73
- H ₂ O - H ₂	%vol %vol	33.89 0.00	29.15 0.00	26.00 0.00	26.07 0.00	22.28 0.00	20.09 0.00	36.85 0.00	30.81 0.00	22.25 0.00	32.26 0.00	31.93 0.00	24.73 0.00
- H ₂ O - H ₂ - CO	%vol %vol %vol	33.89 0.00 0.00	29.15 0.00 0.00	26.00 0.00 0.00	26.07 0.00 0.00	22.28 0.00 0.00	20.09 0.00 0.00	36.85 0.00 0.00	30.81 0.00 0.00	22.25 0.00 0.00	32.26 0.00 0.00	31.93 0.00 0.00	24.73 0.00 0.00

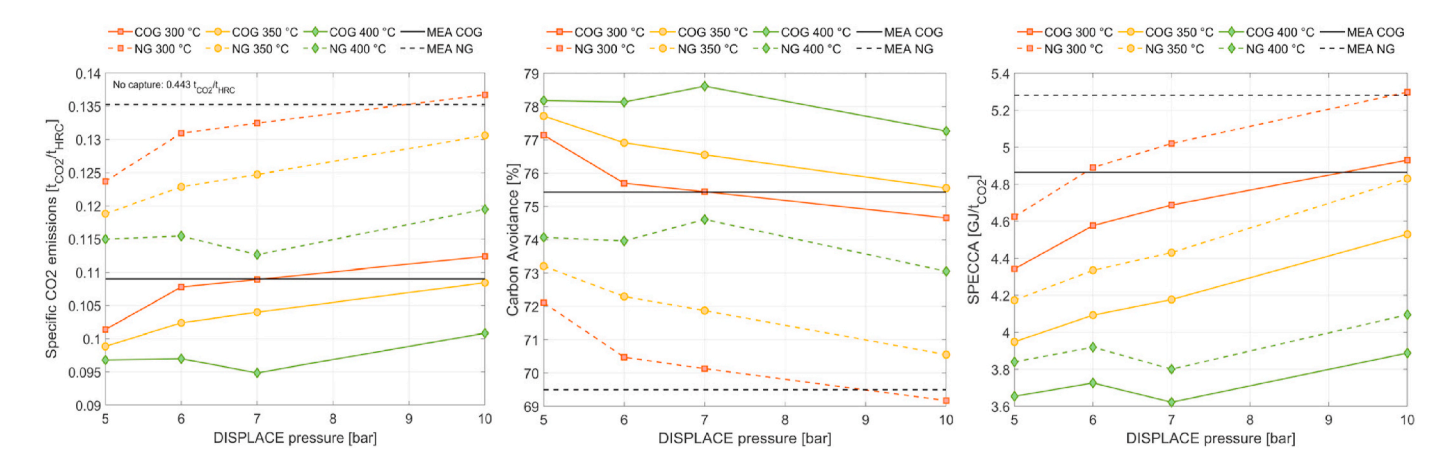


Fig. 10. Specific CO2 emissions, Carbon Avoidance and SPECCA considering both NG and COG as fuels.

rate (CCR) - 90%, 94%, and 98%, as detailed in Table 9. While certain data points in the matrix are absent, specifically all cases where CCR equals 98% and CP equals 97%, along with the case where CCR equals

Table 9 Steam-to-carbon ratio at 400 $^{\circ}\text{C}$ for different working pressures, CP and CCR.

CCR	90%	90%	90%	94%	94%	94%	98%	98%
CP	95%	97%	99%	95%	97%	99%	95%	99%
5 bar	2.30	2.35	2.50	2.43	NA	2.75	2.70	3.37
6 bar	2.26	2.32	2.47	2.40	2.44	2.58	2.68	2.95
7 bar	2.10	2.15	2.42	2.33	2.65	2.71	2.65	3.46
10 bar	2.32	2.40	2.48	2.65	2.73	2.74	3.30	3.25

94% and CP equals 97% at 5 bar, the remaining cases provide sufficient coverage to generate comprehensive results across different CP and CCR values. The general trends are a higher S/C need for higher purity and/or capture rates for each pressure level. The trends between the various pressure levels show a local minimum for 7 bar. This is a consequence of the shape of the isotherm for CO₂ and H₂O respectively. At 7 bar the combination of the CO₂ and steam capacities is the most favourable leading to a low S/C.

To maintain conciseness, Table 9 exclusively presents the steam-to-carbon ratio. Supplementary details pertinent to the simulations are provided in appendix, Table 16, Section 5.3.

 $\begin{tabular}{ll} \textbf{Table 10} \\ \textbf{Results obtained considering the cases of Table 8 and the MEA reference case.} \\ \end{tabular}$

Case	P [bar]	T [°C]	Flue gas compression [MW _e]	CO ₂ Compression [MW _e]	Total Electricity [MW _e]	Fuel consumption [MW _{th}]
1	5	300	16.01	11.38	27.39	125.71
2	5	350	16.01	11.33	27.34	112.49
3	5	400	16.00	11.28	27.28	102.55
4	6	300	17.81	10.30	28.11	130.15
5	6	350	17.81	10.31	28.11	115.31
6	6	400	17.81	10.34	28.15	104.11
7	7	300	19.37	9.53	28.90	132.74
8	7	350	19.37	9.51	28.88	116.80
9	7	400	19.36	9.57	28.93	100.17
10	10	300	23.13	7.80	30.93	137.16
11	10	350	23.13	7.79	30.93	124.97
12	10	400	23.14	7.80	30.94	105.19
MEA	-	-	2.99	16.21	19.20	154.76

Table 11Economic results obtained considering the cases of Table 8, the MEA reference case and NG or COG as fuel.

Case	P [bar]	T [°C]	DISPLACE Capex [M€/y]	Other Capex [M€/y]	Total Capex [M€/y]	Electricity [M€/y]	Fuel [M€/y]	Other costs [M€/y]	LCOHRC $[\ell/t_{HRC}]$	CCA NG [€/t _{CO2}]	CCA COG [€/t _{CO2}]
1	5	300	6.07	21.96	28.03	28.08	51.54	3.60	35.20	110.09	103.17
2	5	350	6.35	21.07	27.43	28.02	46.12	3.45	33.23	102.36	96.66
3	5	400	6.59	20.45	27.04	27.96	42.05	3.33	31.77	96.70	91.84
4	6	300	6.60	22.28	28.88	28.81	53.36	3.79	36.34	116.29	108.59
5	6	350	6.98	21.28	28.26	28.82	47.28	3.60	34.16	106.55	100.40
6	6	400	7.25	20.56	27.81	28.85	42.69	3.45	32.53	99.18	94.10
7	7	300	6.20	22.54	28.74	29.62	54.42	3.71	36.87	118.54	110.48
8	7	350	6.50	21.42	27.93	29.61	47.89	3.53	34.48	108.17	101.79
9	7	400	6.76	20.18	26.94	29.65	41.07	3.35	31.96	96.62	91.89
10	10	300	6.51	22.92	29.44	31.70	56.24	3.89	38.38	125.10	116.20
11	10	350	6.84	22.20	29.04	31.70	51.24	3.71	36.61	117.00	109.52
12	10	400	7.10	20.63	27.72	31.71	43.13	3.45	33.55	103.55	98.13
MEA	-	-	_	-	35.29	19.68	62.05	2.79	37.91	123.00	113.33

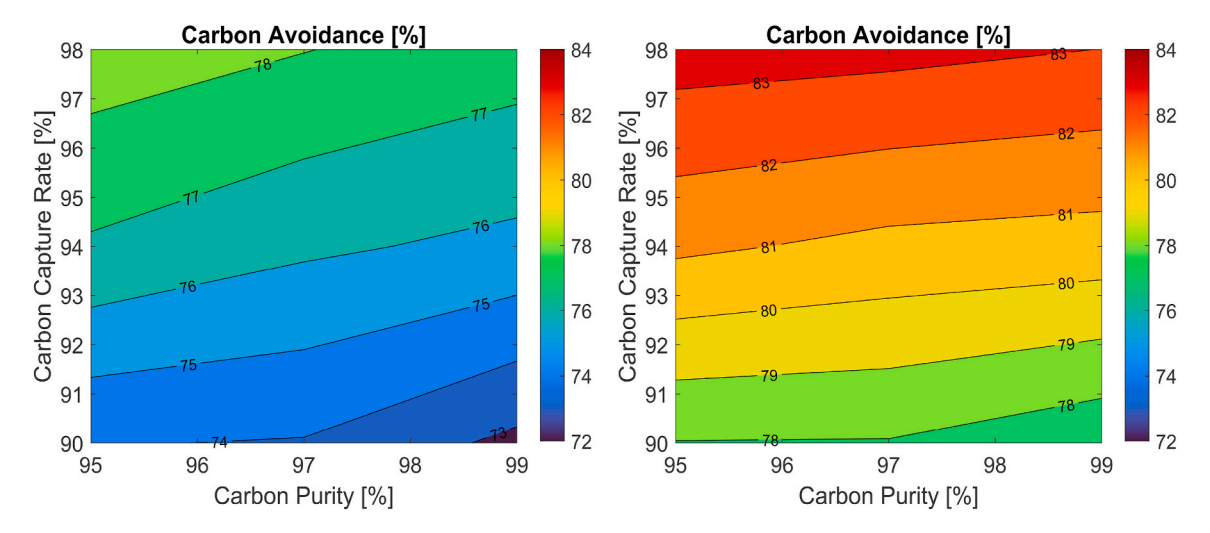


Fig. 11. Carbon avoidance as a function of CP and CCR for cases in Table 9, NG case (left) and COG case (right).

3.2. DISPLACE integration performance

In this section, the main results of the techno-economic assessment for the DISPLACE integration with steel gases are presented and assessed through the KPIs. Table 10 and Table 11 display the comprehensive results obtained for various DISPLACE working pressures and

temperatures, encompassing both NG and COG scenarios. These results are also visually depicted in Fig. 10. Table 10 shows that elevating the DISPLACE operating pressure results in a higher total electricity consumption due to increased power demand by the flue gas compressor. However, the presence of a $\rm CO_2$ -rich stream at the same pressure level as DISPLACE reduces the energy needed for compression to the levels

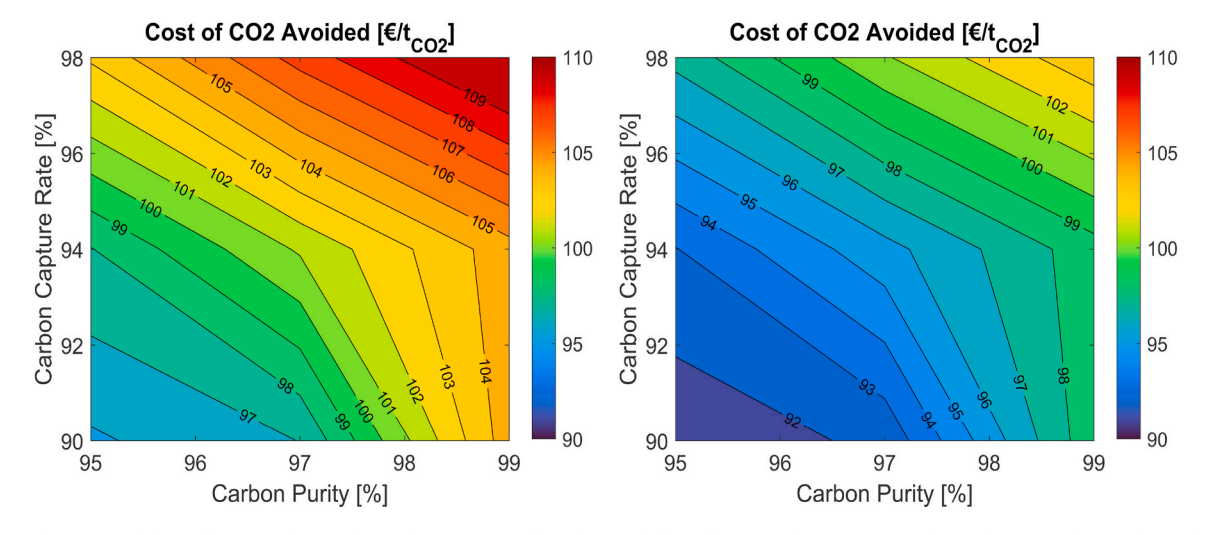


Fig. 12. Cost of CO₂ avoided as a function of CP and CCR for cases in Table 9 for NG (left) and COG (right) case. For each combination of CP and CCR the case with the minimum CCA is selected.

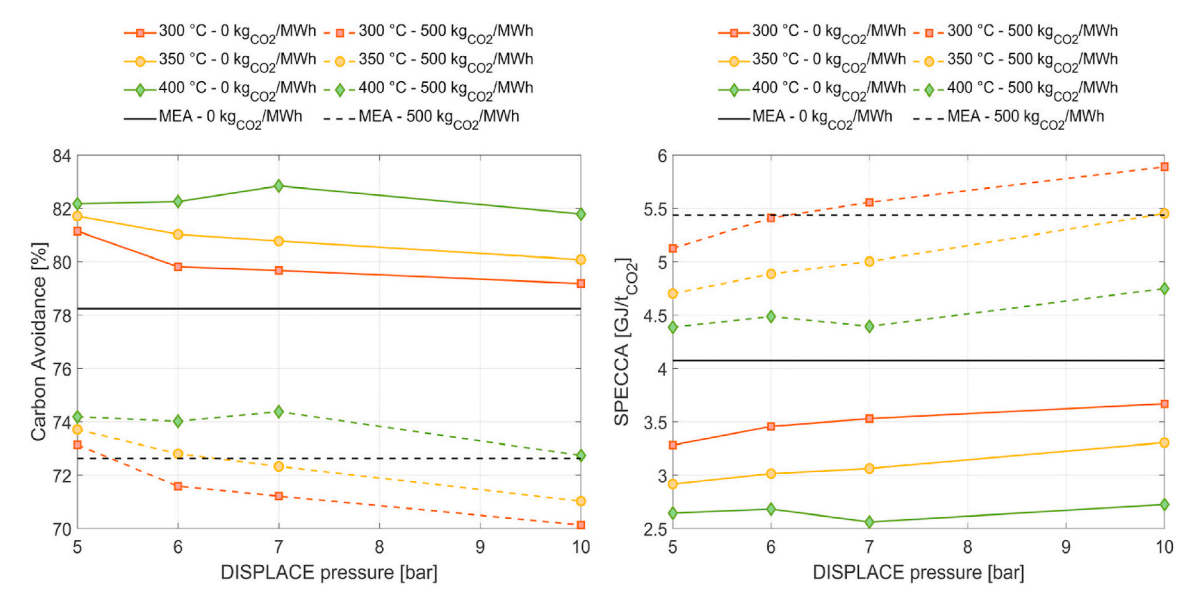


Fig. 13. Carbon Avoidance (left) and SPECCA (right) considering COG as fuel and assuming different carbon footprint of imported electricity (0 kg_{CO2}/MWh and 500 kg_{CO2}/MWh).

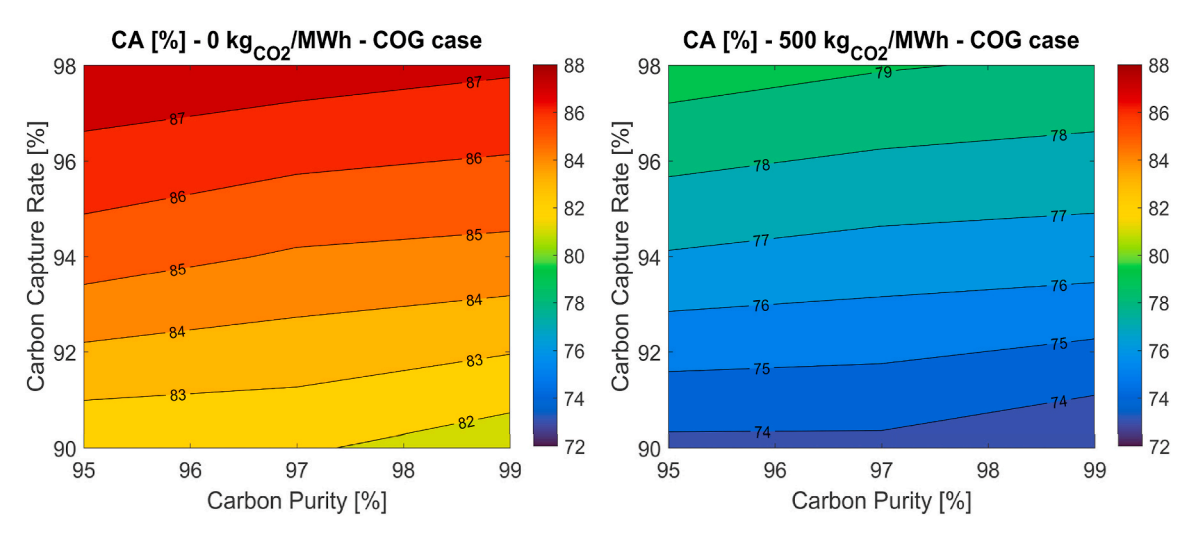
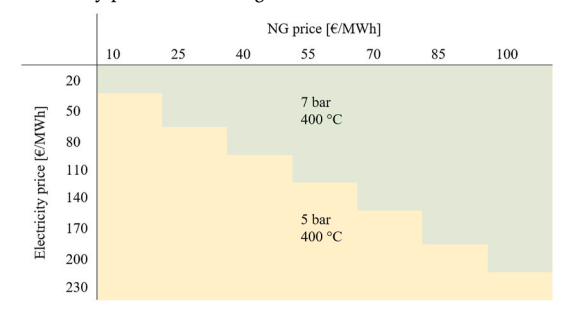


Fig. 14. Carbon avoidance as a function of CP and CCR for cases in Table 9 assuming COG as fuel, for different carbon footprint of imported electricity (0 kg_{CO2}/MWh).

required for transport and storage. This dynamic counteracts the escalating energy demand of the flue gas compressor, thus limiting the overall increase in electricity consumption. Fuel consumption is driven

Table 12Optimal working conditions of DISPLACE for different NG and electricity prices considering both NG and COG as fuel.



by the steam demand, so it increases at lower operating temperature. When utilizing NG as the fuel source to supply the additional heat required for the CO_2 capture process, a carbon avoidance up to 74.6% is achievable (7 bar and 400 $^{\circ}$ C). Generally, elevating the DISPLACE

Table 13 Equipment reference cost.

Component	Scaling parameter	C ₀ [M€]	S ₀	f	Ref.
CO ₂ compressor and condenser	Power, MW	55.24	50.5	0.67	Manzolini et al. (2020)
CO ₂ capture unit (MEA)	CO ₂ mass flow rate, kg/s	85.25	53.7	0.8	Manzolini et al. (2020)
Compressor	Power, MW	10.17	15.3	0.67	Manzolini et al. (2020)
NG Boiler	Heat duty, MW	2.95	10	1	Khallaghi et al. (2022)
Heat exchanger	Heat transfer, MW	16.25	138	0.6	Guo et al. (2014)
Pump	Volumetric flow [m ³ /h]	0.28	250	0.14	Huijgen et al. (2007)

Table 14
Methodology used to compute the total plant cost of the additional equipment (Manzolini et al., 2020).

Cost		Value
Total Installation Cost (TIC)	% TEC	104
Indirect Costs (IC)	% TDPC	14
Contingency (Co)	% EPC	10
Owner's Costs (OC)	% EPC	5

working temperature proves advantageous due to the reduced steam-to-carbon ratio, subsequently minimizing the amount of fuel needed to supply the extra heat. The use of COG offers additional benefits in terms of $\rm CO_2$ avoidance due to its hydrogen-rich composition. The layout of the $\rm C^4U$ steel mill facilitates the utilization of COG, as the absence of a dedicated power plant allows for the utilization of blast furnace gas in certain processes instead of COG, such as slab reheating, thereby enhancing the availability of COG within the steel plant. For this reason, the possibility of using COG was also evaluated.

Comparative analysis with the reference post-combustion MEA process is also presented, with energy consumption of 3.30 GJ/t_{CO2} at the reboiler and a carbon purity of 99.31%. The reboiler heat requirement was assumed to be met through steam generated in a NG/COG fired steam generator. Notably, operating at 400 °C demonstrates a clear advantage for DISPLACE over the MEA process in terms of carbon avoidance. In relation to SPECCA, the DISPLACE exhibits a lower value compared to the MEA case particularly when operating between 350 °C and 400 °C. When considering coke oven gas (COG), the SPECCA is further reduced with respect to the NG case because of the higher carbon avoidance that can be reached.

Focusing on the scenarios operating at 400 $^{\circ}$ C as detailed in section 5.3, Fig. 11 illustrates the carbon avoidance as a function of carbon purity and DISPLACE carbon capture rate, for both the NG an COG cases. An increase in the carbon capture rate (CCR) allows for higher carbon avoidance levels, while a shift towards elevated carbon purity values amplifies the DISPLACE steam-to-carbon ratio, thereby reducing the overall carbon avoidance as the additional steam has to be produced through a NG/COG fired steam generator.

Table 11 shows the economic outcomes: at the same operating temperature, an increase in operating pressure leads to a rise in DISPLACE capital expenditure. However, higher pressure allows for a reduction in column radius, thereby partially mitigating this effect. Consequently, transitioning from 6 to 7 bar, the DISPLACE capital cost decreases. When maintaining the same operating pressure, DISPLACE capital expenditure increases with temperature, while additional equipment costs exhibit the opposite trend. This results in a trend with

Table 15 Number of valves per column.

Valve	N° valves
Feed valve	1
Recycle valve	2
CO ₂ product valve	1
Lean product valve	1
Steam valve	1

minor fluctuations in capital costs. Conversely, operating costs are more influenced by DISPLACE operating conditions, aligning with trends in electricity and fuel consumption. The adoption of DISPLACE proves advantageous compared to the reference MEA scrubbing, particularly in cases operating at 350 and 400 °C. It is important to emphasize the difference in TRL between the two technologies, which leads to greater uncertainty regarding the performance and cost of DISPLACE technology when evaluating its potential at an industrial scale. As mentioned earlier, MEA scrubbing is a mature technology that has already been proven on an industrial scale. Nevertheless, the estimation of the MEA carbon capture section's CAPEX was derived from literature sources and, as such, carries inherent uncertainties. The adoption of COG reduces the cost of CO₂ avoided because of the higher carbon avoidance. For scenarios operating at 400 °C (Table 9), the cost of CO₂ avoided is computed while varying CP and DISPLACE CCR (see Fig. 12). The increase of CCA is the consequence of the higher steam-to-carbon ratio demanded by DISPLACE when shifting towards higher values of CP and CCR. For the same reason described before, the COG case shows lower values of CCA.

3.2.1. Sensitivity on carbon footprint of imported electricity

The carbon footprint of imported electricity significantly impacts the overall CA together with SPECCA. The impact of carbon footprint of imported electricity set at 0 kgCO2/MWh, and 500 kgCO2/MWh are depicted in Fig. 13, alongside the reference MEA case for comparison. Under the renewable energy scenario (0 kgCO2/MWh) and utilizing COG, it is possible to reach a carbon avoidance above 82% and a SPECCA close

 Table 16

 Assumptions for the DISPLACE economic assessment.

Cost		Value
Construction works	% C _{colums}	170
Other costs	% TEC + C _{costruction}	3.5
EPCM services	% TDC _{DISPLACE}	17.5
Contingency	$\mathrm{TDC}_{\mathrm{DISPLACE}} + \mathrm{EPCM}$	15

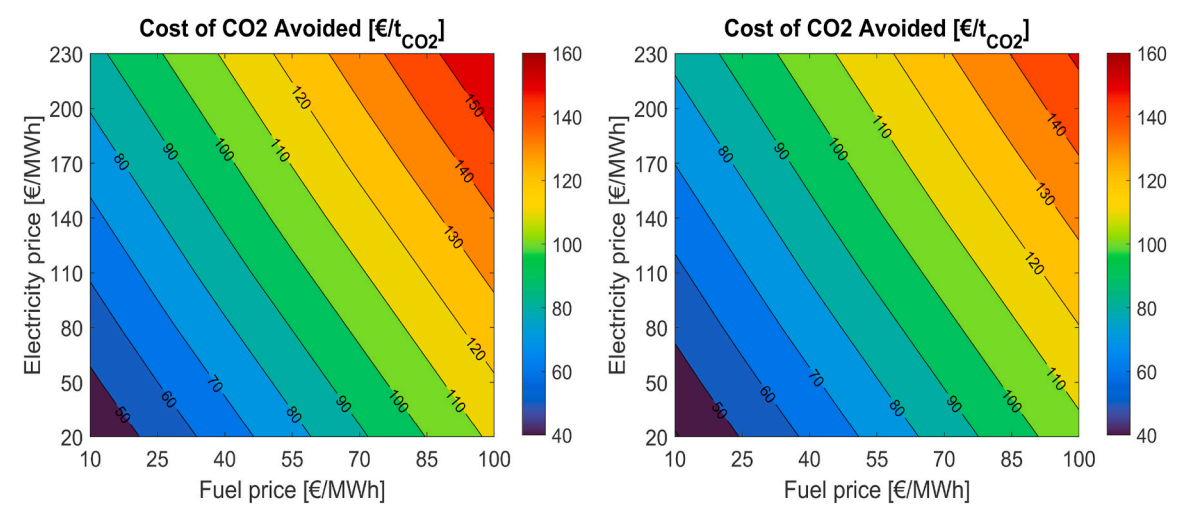


Fig. 15. Cost of CO₂ avoided as function of fuel and electricity prices for the NG case (left) and for COG case (right).

to 2.5 GJ/t_{CO2}, which is significantly lower than the MEA case. These trends can be extended to the NG case with a reduction of CA by around 4–6% points and an increase in SPECCA by 0.2–0.5 MJ/kg_{CO2}. Fig. 14 illustrates carbon avoidance as a function of CP and DISPLACE CCR for cases operating at 400 °C (Table 9): the highest value of carbon avoidance (higher than 87%) is reached for CCR = 98%, CP = 95% in the renewable energy scenario using COG as additional fuel.

3.2.2. Sensitivity on natural gas and electricity price

The economic outcomes are significantly influenced by the prices of electricity and NG. Given the considerable uncertainty associated with these factors, a sensitivity analysis is conducted. The results shown in this section are referred to the cases listed in Table 8. For each combination of NG and electricity prices outlined in Table 12, the corresponding DISPLACE working temperature and pressure that minimize the CCA are identified. At low NG prices and escalating electricity costs, the 5 bar pressure – 400 °C temperature combination becomes the most cost-effective option because of the lower overall power consumption at 5 bar pressure, resulting in savings in electricity procurement. Conversely at higher NG prices the best combination results to be 7 bar–400 °C due to the reduced DISPLACE steam-to-carbon ratio.

Fig. 15 illustrate the cost of ${\rm CO_2}$ avoidance against fuel and electricity prices. The utilization of COG allows for reduced CCA values, owing to the enhanced carbon avoidance achievable with COG.

4. Conclusion

This article introduces the innovative DISPLACE carbon-capture technology, which is based on adsorption of $\rm CO_2$ and steam on solid materials. In particular, the feasibility of utilizing DISPLACE for decarbonizing exhaust gases emitted from the hot-stoves in a BF-BOF steel plant is thoroughly analysed.

The DISPLACE technology is a multi-column, cyclic, concentration swing process operated isobarically for the capture of CO₂. Carbon capture rates (CCR) of up to 98% and (dry) CO₂ purities (CP) of up to 99% can be achieved. The benefits of the system are the low temperature variation due to similar heat of adsorption between the two adsorbing species and the low fatigue of the unit due to the isobaric operation. The major trade-offs of the system were identified as the performance (CP and CCR) vs steam demand, system temperature vs steam demand and system pressure vs productivity/system size. As the system pressure requires feed pressurisation but also produces higher pressure CO₂, the choice of the final design is not only a technical one but also impacted by the integration option based on available heat sources and downstream units and unit size vs energy consumption decision.

The integration of DISPLACE technology into a steel mill layout was performed using Aspen Plus V14. An optimization process was conducted on two crucial DISPLACE design parameters: operating temperature and pressure. These parameters significantly influence the steam required for the DISPLACE carbon capture system. Results demonstrated a distinct advantage in operating at 400 °C due to reduced steam consumption for the DISPLACE technology, leading to lower energy penalties associated with steam generation. Two different fuels, NG and

COG, were evaluated to fulfil the process heat requirement. Additionally, a benchmark post-combustion carbon capture technology based on MEA scrubbing was modelled and compared to DISPLACE. Key performance indicators (KPIs) revealed the superiority of DISPLACE over MEA especially when operating at 400 $^{\circ}$ C.

In the renewable energy scenario, the best case resulted in achieving over 82% carbon avoidance and a SPECCA close to 2.5 GJ/t_{CO2}. From an economic perspective, the cost of avoided CO₂ was found to be 91.89 $\rm \ell/t_{CO2}$ for 7 bar–400 °C using COG, or 96.62 $\rm \ell/t_{CO2}$ when using imported NG. In both cases, the cost associated with DISPLACE process was significantly lower compared to the MEA case (equal to 113.33.42 $\rm \ell/t_{CO2}$ and 123.00 $\rm \ell/t_{CO2}$ respectively).

In conclusion, DISPLACE technology emerges as a promising solution for decarbonizing processes within BF-BOF steel mills, with the potential for significant emissions reduction in this industrial sector.

Future works will investigate the optimal integration of DISPLACE within integrated steelworks considering different exhaust gases as the ones from sinter plant or reheating ovens, including the optimal integration to minimize the additional impact will be identified. Separately, experimental results and model validation will be detailed.

CRediT authorship contribution statement

Nicola Zecca: Writing – original draft, Visualization, Methodology, Investigation, Formal analysis, Conceptualization. Leonie Lücking: Writing – original draft, Visualization, Validation, Methodology, Investigation, Formal analysis, Conceptualization. Dora-Andreea Chisăliță: Investigation, Formal analysis. Jurriaan Boon: Writing – review & editing, Validation, Methodology. H.A.J. van Dijk: Writing – review & editing, Supervision, Funding acquisition, Conceptualization. J.A.Z. Pieterse: Project administration, Funding acquisition. Antonio Giuffrida: Project administration, Funding acquisition. Giampaolo Manzolini: Writing – review & editing, Supervision, Methodology, Funding acquisition, Conceptualization.

Declaration of competing interest

The authors declare the following financial interests/personal relationships which may be considered as potential competing interests: Jurriaan Boon has patent #WO2022053676A1 issued to TNO. If there are other authors, they declare that they have no known competing financial interests or personal relationships that could have appeared to influence the work reported in this paper.

Acknowledgements

This paper is part of the C^4U project that has received funding from the European Union's Horizon 2020 research and innovation programme under grant agreement N°884418.

The work reflects only the authors' views, and the European Union is not liable for any use that may be made of the information contained therein.

Appendix

Streams specifications of DISPLACE plant integration

In Table 13 the specifications of the streams indicated in Fig. 5 are given. Since many cases were analysed, for sake of brevity results referring to the 5 bar–400 $^{\circ}$ C case are presented.

Table 13 Main streams specifications of DISPLACE plant integration. Case 5 bar–400 $^{\circ}\text{C.s}$

Stream	Temperature	Pressure	Mass flow rate	Composit	tion [%mo	1]							
	[°C]	[bar]	[kg/s]	H ₂ O	H ₂	CO	CO_2	N ₂	O_2	CH ₄	C ₂ H ₆	C ₃ H ₈	C ₅ H ₁₂
1	140.0	1.1	87.9	6.2	_	-	41.9	50.8	1.0	-	-	-	-
2	35.0	0.9	87.9	6.2	_	_	41.9	50.8	1.0	_	_	_	_
3	400.0	5.0	87.1	4.7	_	_	42.6	51.6	1.0	_	_	_	_
4	399.1	4.8	78.8	60.3	_	_	3.0	36.0	0.7	_	_	_	_
5	126.9	4.0	78.8	60.3	_	_	3.0	36.0	0.7	_	_	_	_
6	400.0	4.8	50.7	26.0	_	_	70.6	3.3	_	_	_	_	_
7	34.9	110.0	43.0	0.3	_	_	95.3	4.4	_	_	_	_	_
8	20.0	1.2	2.2	_	_	_	1.8	0.4	_	83.9	9.2	3.3	1.2
9	15.0	1.0	41.6	_	_	_	_	79.0	21.0	_	_	_	_
10	99.9	1.0	43.8	15.4	0.1	0.1	8.5	72.5	3.0	_	_	_	_
11	15.0	1.0	42.9	100.0	_	_	_	_	_	_	_	_	_
12	102.0	1.3	2.2	100.0	_	_	_	_	_	_	_	_	_
13	102.0	1.3	30.1	100.0	_	_	_	_	_	_	_	_	_
14	102.0	1.3	10.6	100.0	_	_	_	_	_	_	_	_	_
15	107.2	7.2	43.3	100.0	_	_	_	_	_	_	_	_	_
16	157.5	5.8	6.6	100.0	_	_	_	_	_	_	_	_	_
17	157.5	5.8	13.2	100.0	_	_	_	_	_	_	_	_	_
18	157.5	5.8	23.2	100.0	_	_	_	_	_	_	_	_	_
19	400.0	5.4	42.4	100.0	_	_	_	_	_	_	_	_	_
20	152.9	4.5	0.5	100.0	_	-	_	-	-	_	_	_	-

MEA post-combustion carbon capture modelling

Details about the CHEMESTRY and the REACTION Aspen Plus models used to simulate the MEA carbon capture system are presented in this section.

CHEMISTRY model:

Equilibrium	$MEA^+ + H_2O{\rightleftharpoons}MEA + H_3O^+$	(21)
Equilibrium	$MEACCO^- + H_2O \rightleftharpoons MEA + HCO_3^-$	(22)
Equilibrium	$CO_2 + 2H_2O \rightleftharpoons H_3O^+ + HCO_3^-$	(23)
Equilibrium	$HCO_3^- + H_2O \rightleftharpoons H_3O^+ + CO_3^{2-}$	(24)
Equilibrium	$2H_2O\rightleftharpoons H_3O^+ + OH^-$	(25)

The equilibrium constant of the reactions (21)–(25) is calculated adopting equation (26) with the constants listed in Table 14.

$$\ln(K_{eq}) = A + B/T + C \cdot \ln(T) + D \cdot T + E \cdot \left(\left(P - P_{ref} \right) / P_{ref} \right)$$
(26)

Table 14
Constants used in equation (26).

Reaction	A	В	C	D	E
$MEA^+ + H_2O \rightleftharpoons MEA + H_3O^+$	-3.038325	-7008.36	0	-0.00313489	0
$MEACCO^- + H_2O \rightleftharpoons MEA + HCO_3^-$	-0.52135	-2545.53	0	0	0
$CO_2 + 2H_2O \rightleftharpoons H_3O^+ + HCO_3^-$	231.465	-12092.1	-36.7816	0	0
$HCO_3^- + H_2O \rightleftharpoons H_3O^+ + CO_3^{2-}$	216.049	-12431.7	-35.4819	0	0
$2H_2O\rightleftharpoons H_3O^+ + OH^-$	132.899	-13445.9	-22.4773	0	0

REACTION model:

Equilibrium	$MEA^+ + H_2O{\rightleftharpoons}MEA + H_3O^+$	(27)
Equilibrium	$2H_2O\rightleftharpoons H_3O^+ + OH^-$	(28)
Equilibrium	$HCO_3^- + H_2O \rightleftharpoons H_3O^+ + CO_3^{2-}$	(29)
Kinetic	$CO_2 + OH^- \rightleftharpoons HCO_3^-$	(30)
Kinetic	$HCO_3^- \rightleftharpoons CO_2 + OH^-$	(31)
Kinetic	$MEA + CO_2 + H_2O \rightleftharpoons MEACCO^- + H_3O^+$	(32)
Kinetic	$MEACCO^- + H_3O^+ \rightleftharpoons MEA + CO_2 + H_2O$	(33)

The power law expressions are used for the rate-controlled reactions:

$$r = kT^n \exp\left(-\frac{E}{RT}\right) \prod_{i=1}^{N} \left(x_i \gamma_i\right)^{a_i} \tag{34}$$

Where: r = rate of reaction; k = pre-exponential factor; T = absolute temperature; n = temperature exponent; E = activation energy; R = universal gas constant; N = number of components in the reaction; $x_i = mole$ fraction of component i; $\gamma_i = activity$ coefficient of component i; $a_i = stoichiometric$ coefficient of component i in the reaction equation.

In equation (34), the factor n is zero, k and E are given in Table 15.

Table 15 Parameters used in equation (34).

Reaction	k	E [cal/mol]
$CO_2 + OH^- \rightleftharpoons HCO_3^-$	1.33e+17	13249
$HCO_3^- \rightleftharpoons CO_2 + OH^-$	6.63e + 16	25656
$MEA + CO_2 + H_2O \rightleftharpoons MEACCO^- + H_3O^+$	3.02e+14	9855.8
$MEACCO^- + H_3O^+ \rightleftharpoons MEA + CO_2 + H_2O$	5.52e + 23	16518

DISPLACE performances at 400 °C

Table 16 shows the performances of DISPLACE when operating at 400 °C and for different values of CP and CCR.

Table 16 DISPLACE performances for the cases at 400 °C.

Case	Unit	1	2	3	4	5	6	7	8	9	10	11	12
P	bar	5	5	5	5	5	5	5	6	6	6	6	6
Γ	°C	400	400	400	400	400	400	400	400	400	400	400	400
D	m	3	3	3	3	3	3	3	3	3	3	3	3
CP	%	95.69	97.06	98.69	95.40	98.57	94.83	99.22	95.44	97.33	98.63	94.79	97.2
CCR	%	90.33	90.22	89.94	94.37	94.03	97.89	97.64	89.64	90.28	90.01	94.38	93.9
S/C	mol/mol	2.30	2.35	2.50	2.43	2.75	2.70	3.37	2.26	2.32	2.47	2.40	2.4
CO ₂ stream	kmol/s	1.54	1.53	1.54	1.74	1.91	2.14	2.61	1.31	1.34	1.41	1.61	1.5
CO ₂ -rich strea	m composition	at reactor o	utlet										
- Ar	%vol	0.06	0.04	0.02	0.06	0.02	0.05	0.01	0.07	0.04	0.02	0.07	0.0
- H ₂ O	%vol	33.71	34.41	36.27	38.75	46.02	48.04	59.31	22.80	25.13	30.21	33.20	33.9
- H ₂	%vol	0.00	0.00	0.00	0.00	0.00	0.00	0.00	0.00	0.00	0.00	0.00	0.0
- CO	%vol	0.00	0.00	0.00	0.00	0.00	0.00	0.00	0.00	0.00	0.00	0.00	0.0
- CO ₂	%vol	63.43	63.67	62.89	58.44	53.21	49.27	40.38	73.67	72.87	68.84	63.32	64.2
- N ₂	%vol	2.80	1.89	0.82	2.76	0.76	2.63	0.31	3.45	1.96	0.94	3.41	1.7
- O ₂	%vol	0.00	0.00	0.00	0.00	0.00	0.00	0.00	0.00	0.00	0.00	0.00	0.0
Case	Unit	13	14	15	16	17	18	19	20	21	22	23	24
P	bar	6	6	6	7	7	7	7	7	7	7	7	10
T	°C	400	400	400	400	400	400	400	400	400	400	400	400
D	m	3	3	3	2.75	2.75	2.75	2.75	2.75	2.75	2.75	2.75	2.5
CP	%	98.96	95.29	98.70	95.32	96.94	98.55	95.31	96.86	98.74	95.43	98.85	95.3
CCR	%	94.29	97.80	98.13	89.97	90.12	90.37	94.12	94.23	93.63	97.60	97.72	89.9
S/C	mol/mol	2.58	2.68	2.95	2.10	2.15	2.42	2.33	2.65	2.71	2.65	3.46	2.3
CO ₂ stream	kmol/s	1.61	1.97	2.04	1.35	1.36	1.50	1.65	1.89	1.83	2.07	2.72	1.4
CO ₂ -rich strea	m composition	at reactor o	utlet										
- Ar	%vol	0.01	0.05	0.01	0.07	0.05	0.02	0.06	0.04	0.01	0.05	0.02	0.0
- H ₂ O	%vol	36.03	43.76	47.40	24.72	26.28	34.06	35.58	44.37	44.19	46.60	60.73	29.0
- H ₂	%vol	0.00	0.00	0.00	0.00	0.00	0.00	0.00	0.00	0.00	0.00	0.00	0.0
- CO	%vol	0.00	0.00	0.00	0.00	0.00	0.00	0.00	0.00	0.00	0.00	0.00	0.0
- CO ₂	%vol	63.31	53.58	51.92	71.75	71.47	64.98	61.40	53.88	55.11	50.95	38.82	67.6
- N ₂	%vol	0.65	2.60	0.67	3.46	2.21	0.94	2.96	1.71	0.69	2.39	0.43	3.2
- O ₂	%vol	0.00	0.00	0.00	0.00	0.00	0.00	0.00	0.00	0.00	0.00	0.00	0.0
Case	Uni	it	25		26	27		28		29	30		31
P	bar		10		10	10		10		10	10		10
T	°C		400		400	400		400		400	400		400
D	m		2.5		2.5	2	2.5	2.5		2.5	2.5	5	2.5
CP	%		97.12		98.73		5.37	97.28		98.79	95.0	07	98.9
CCR	%		90.41		90.39	94	1.27	93.86		93.98	97.	55	98.1
S/C	mo	l/mol	2.40		2.48	2	2.65	2.73		2.74	3.3	30	3.2
CO ₂ stream	km	ol/s	1.48		1.37		1.91	1.87		1.66	2.0		2.2
CO ₂ -rich strea	m composition	at reactor o	utlet										
- Ar	%ve	ol	0.04		0.02	(0.05	0.03		0.02	0.0	04	0.0

(continued on next page)

Table 16 (continued)

Case	Unit	25	26	27	28	29	30	31
- H ₂ O	%vol	32.19	27.70	44.14	44.42	38.07	58.19	52.59
- H ₂	%vol	0.00	0.00	0.00	0.00	0.00	0.00	0.00
- CO	%vol	0.00	0.00	0.00	0.00	0.00	0.00	0.00
- CO ₂	%vol	65.86	71.38	53.27	54.07	61.19	39.75	46.90
- N ₂	%vol	1.91	0.90	2.53	1.48	0.73	2.02	0.50
- O ₂	%vol	0.00	0.00	0.00	0.00	0.00	0.00	0.00

Capital cost estimation procedure

In the case of the MEA post-combustion carbon capture section the methodology described in Section 2.2.5 has been adopted using the values listed in Table 15 and in Table 13 along with equations (35)–(41). The reference values found in literature and used to carry out the economic assessment have been updated through the CEPCI index computed as the average between the years 2019 and 2022. Therefore the CEPCI index used in this work is equal to 712.47 and the resulting values are shown in Table 14 (in column " C_0 ").

$$C_{e,i} = n \cdot C_{0,i} \left(\frac{S_{e,i}}{n \cdot S_{0,i}} \right)^f$$
(35)

$$TEC = \sum_{i=1}^{n} C_{e,i}$$

$$(36)$$

$$TDPC = TEC + TIC \tag{37}$$

$$EPC = TDPC + IC$$
 (38)

$$TPC = EPC + Co + OC$$
(39)

$$FCF = \frac{r(1+r)^n}{(1+r)^n - 1} \tag{40}$$

$$TAC\left[\frac{M\ell}{y}\right] = TPC \cdot FCF + C_{el} + C_{NG} + C_{H_2O} + C_f + C_{O\&M}$$
(41)

In the case of the DISPLACE technology, the following methodology was adopted. The steel selected to manufacture the DISPLACE is carbon steel P355GH. Regarding the economic assessment of the additional equipment necessary to be installed for the carbon capture process through the DISPLACE technology (i.e. compressors, pumps, etc.) the methodology described for the MEA carbon capture section was used with the values listed in Table 14. Equations (42)–(70) were used to compute the DISPLACE total plant cost.

$$T_{\text{design}}[^{\circ}C] = T_{\text{woking}} + 30 \tag{42}$$

$$P_{\text{design}}[\text{bar}] = P_{\text{woking}} + 2.2 \tag{43}$$

$$f_{d}[MPa] = min\left(\frac{R_{p0.2/T}}{1.5}; \frac{R_{m/20}}{2.4}\right) \tag{44}$$

$$R_{p0.2/T}[MPa] = 0.0007 \cdot T_{design}^2 - 0.7794 \cdot T_{design} + 403.69$$
 (45)

$$R_{m/20}[MPa] = 510$$
 (46)

$$z[mm] = 0.85 \tag{47}$$

$$CA[mm] = 3.00 \tag{48}$$

$$t_{\text{wall}}[mm] = \frac{P_{\text{design}}/10 \cdot D_e \cdot 1000}{2 \cdot f_d \cdot z + P_{\text{design}}/10} \tag{49}$$

$$t_{\text{hemispherical head}}[mm] = \frac{P_{\text{design}}/10 \cdot D_{\text{column}} \cdot 1000}{4 \cdot f_{\text{d}} \cdot z + P_{\text{design}}/10} \tag{50}$$

$$SF = 1.50$$
 (51)

$$t_{\text{vessel wall}} [\text{mm}] = t_{\text{wall}} \cdot \text{SF} + \text{CA}$$
 (52)

$$t_{\text{vessel head}} [\text{mm}] = t_{\text{hemispherical head}} \cdot \text{SF} + \text{CA}$$
 (53)

$$D_{i}[m] = D_{e} - 2 \cdot t_{vessel\ wall} \tag{54}$$

$$V_{\text{vessel}}[m^3] = \pi/4 \cdot (D_a^2 - D_i^2) \cdot H$$
 (55)

$$V_{\text{hemispherical head}}\left[m^{3}\right] = 4\left/3\pi\cdot\left(\left(D_{e}/2\right)^{3} - \left(D_{e}/2 - t_{\text{vessel head}}/1000\right)^{3}\right) \tag{56}$$

$$m_{\text{column}}[kg] = 7850 \left[kg/m^{3} \right] \cdot \left(V_{\text{vessel}} + V_{\text{hemispherical head}} \right)$$
(57)

$$c_{\text{columns}}[\epsilon] = c_{\text{steel}}[\epsilon/kg] \cdot m_{\text{column}} \cdot n_{\text{column}} \cdot n_{\text{train}}$$
 (58)

In addition the costs of the valves and of the sorbent have been taken into consideration.

$$v_{\text{max}}[\text{m}/\text{s}] = \sqrt{122/\rho_{\text{gas}}} \tag{59}$$

$$v[m/s] = 5 \tag{60}$$

$$v[m/s] = v_{max} - v_A \tag{61}$$

$$\dot{V}_{gas}[m^3/s] = \frac{\dot{m}_{in}}{2 \cdot \rho_{gas} \cdot n_{train}}$$
(62)

$$A_{\text{valve}}[m^2] = \dot{V}_{gas} / v \tag{63}$$

$$D_{\text{valve}}[m] = 2\sqrt{A_{\text{valve}}/\pi} \tag{64}$$

$$c_{\text{valve}}[\epsilon] = 10000 + 2500 \cdot (2 \cdot \text{round_up}(D_{\text{valve}}/0.025/2))$$
 (65)

$$c_{\text{valves}}[\epsilon] = \sum_{i=1}^{n} \left(c_{\text{valve},i} \cdot n_{\text{valves per column},i} \cdot n_{\text{colums per train}} \cdot n_{\text{train}} \right)$$
(66)

The quantity of valves per each vessel is shown in Table 16.

The total plant cost of the DISPLACE columns and valves is computed with the following equations and the assumptions listed in Table 16.

$$TEC_{DISPLACE}[\epsilon] = c_{columns} + c_{bulk material and freight} + c_{valves}$$
(67)

$$c_{\text{bulk material and freight}}[\epsilon] = 0.77 \cdot c_{\text{columns}}$$
 (68)

$$TDC_{DISPLACE}[\epsilon] = TEC_{DISPLACE} + c_{construction} + c_{other}$$
(69)

$$TPC_{DISPLACE}[\epsilon] = TDC_{DISPLACE} + EPCM_{services} + c_{contingency}$$
(70)

Data availability

The data that has been used is confidential.

References

- Arasto, A., Tsupari, E., Kärki, J., Lilja, J., Sihvonen, M., 2014. Oxygen blast furnace with CO2 capture and storage at an integrated steel mill—Part I: technical concept analysis. Int. J. Greenh. Gas Control 30, 140–147. https://doi.org/10.1016/j.iigec.2014.09.004.
- Baker, R.W., Freeman, B., Kniep, J., Huang, Y.I., Merkel, T.C., 2018. CO2 capture from Cement plants and steel mills using membranes. Ind. Eng. Chem. Res. 57, 15963–15970. https://doi.org/10.1021/acs.iecr.8b02574.
- Biermann, M., Ali, H., Sundqvist, M., Larsson, M., Normann, F., Johnsson, F., 2019. Excess heat-driven carbon capture at an integrated steel mill – considerations for capture cost optimization. Int. J. Greenh. Gas Control 91, 102833. https://doi.org/10.1016/j.ijegc.2019.102833.
- Boon, J., 2023. Sorption-enhanced reactions as enablers for CO2 capture and utilisation. Curr Opin Chem Eng 40, 100919. https://doi.org/10.1016/j.coche.2023.100919.
- Boon, J., Cobden, P.D., van Dijk, H.A.J., Hoogland, C., van Selow, E.R., van Sint Annaland, M., 2014. Isotherm model for high-temperature, high-pressure adsorption of CO2 and H2O on K-promoted hydrotalcite. Chem. Eng. J. 248, 406–414. https:// doi.org/10.1016/J.CEJ.2014.03.056.
- Boon, J., Cobden, P.D., van Dijk, H.A.J., van Sint Annaland, M., 2015. High-temperature pressure swing adsorption cycle design for sorption-enhanced water-gas shift. Chem. Eng. Sci. 122, 219–231. https://doi.org/10.1016/J.CES.2014.09.034.
- C4U website n.d. https://c4u-project.eu/. (Accessed 12 November 2024).
- Chisalita, D.-A., Petrescu, L., Cobden, P., van Dijk Haj Eric, Cormos, A.-M., Cormos, C.-C., 2019. Assessing the environmental impact of an integrated steel mill with postcombustion CO2 capture and storage using the LCA methodology. J. Clean. Prod. 211, 1015–1025. https://doi.org/10.1016/j.jclepro.2018.11.256.
- Chung, W., Roh, K., Lee, J.H., 2018a. Design and evaluation of CO2 capture plants for the steelmaking industry by means of amine scrubbing and membrane separation. Int. J. Greenh. Gas Control 74, 259–270. https://doi.org/10.1016/j.ijggc.2018.05.009.

- Chung, W., Roh, K., Lee, J.H., 2018b. Design and evaluation of CO2 capture plants for the steelmaking industry by means of amine scrubbing and membrane separation. Int. J. Greenh. Gas Control 74, 259–270. https://doi.org/10.1016/j.ijggc.2018.05.009.
- Coenen, K., Gallucci, F., Pio, G., Cobden, P., van Dijk, E., Hensen, E., et al., 2017. On the influence of steam on the CO2 chemisorption capacity of a hydrotalcite-based adsorbent for SEWGS applications. Chem. Eng. J. 314, 554–569. https://doi.org/ 10.1016/j.cei.2016.12.013.
- Coenen, K., Gallucci, F., Hensen, E., van Sint Annaland, M., 2018a. CO2 and H2O chemisorption mechanism on different potassium-promoted sorbents for SEWGS processes. J. CO2 Util. 25, 180–193. https://doi.org/10.1016/j.jcou.2018.04.002.
- Coenen, K., Gallucci, F., Mezari, B., Hensen, E., van Sint Annaland, M., 2018b. An in-situ IR study on the adsorption of CO2 and H2O on hydrotalcites. J. CO2 Util. 24, 228–239. https://doi.org/10.1016/j.jcou.2018.01.008.
- Cormos, C.-C., 2016. Evaluation of reactive absorption and adsorption systems for post-combustion CO2 capture applied to iron and steel industry. Appl. Therm. Eng. 105, 56–64. https://doi.org/10.1016/j.applthermaleng.2016.05.149.
- Cormos, A.-M., Dragan, S., Petrescu, L., Sandu, V., Cormos, C.-C., 2020. Technoeconomic and environmental evaluations of decarbonized fossil-intensive industrial processes by reactive absorption & adsorption CO2 capture systems. Energies 13. https://doi.org/10.3390/en13051268.
- European Commission, 2024. Communication from the Commission to the European Parliament, the Council, the European Economic and Social Committee and the Committee of the Regions: towards an Ambitious Industrial Carbon Management for the EU (Report COM/2024/62 Final).
- Fernández, J.R., Martínez, I., Abanades, J.C., Romano, M.C., 2017. Conceptual design of a Ca–Cu chemical looping process for hydrogen production in integrated steelworks. Int. J. Hydrogen Energy 42, 11023–11037. https://doi.org/10.1016/j.ijhydene.2017.02.141.
- Fernández, J.R., Spallina, V., Abanades, J.C., 2020. Advanced packed-bed Ca-Cu looping process for the CO2 capture from steel mill off-gases. Front. Energy Res. 8. https://doi.org/10.3389/fenrg.2020.00146.
- Gazzani, M., Romano, M.C., Manzolini, G., 2015. CO2 capture in integrated steelworks by commercial-ready technologies and SEWGS process. Int. J. Greenh. Gas Control 41, 249–267. https://doi.org/10.1016/j.ijggc.2015.07.012.
- Guo, Z., Wang, Q., Fang, M., Luo, Z., Cen, K., 2014. Thermodynamic and economic analysis of polygeneration system integrating atmospheric pressure coal pyrolysis

- technology with circulating fluidized bed power plant. Appl. Energy 113, 1301–1314. https://doi.org/10.1016/j.apenergy.2013.08.086.
- Helfferich, F.G., 1984. In: Ruthven, D.M. (Ed.), Principles of Adsorption & Adsorption Processes, vol. 31. John Wiley & Sons, pp. 523–524. https://doi.org/10.1002/ aic.690310335 xxiv + 433 pp. AIChE Journal 1985.
- Huijgen, W.J.J., Comans, R.N.J., Witkamp, G.-J., 2007. Cost evaluation of CO2 sequestration by aqueous mineral carbonation. Energy Convers. Manag. 48, 1923–1935. https://doi.org/10.1016/j.enconman.2007.01.035.
- IEAGHG Technical Report, 2013. Iron and Steel CCS Study (Techno-Economics Integrated Steel Mill).
- International Energy Agency, 2020. Iron and Steel Technology Roadmap towards More Sustainable Steelmaking Part of the Energy Technology Perspectives Series.
- International industrial energy prices GOV.UK n.d. https://www.gov.uk/government/s tatistical-data-sets/international-industrial-energy-prices (accessed April 10, 2024).
- Jeon, J.-Y., Park, B.-R., Kim, J.-H., 2022. Numerical simulation and optimization of 4component LDG separation in the steelmaking industry using polysulfone hollow fiber membranes. Membranes 12. https://doi.org/10.3390/membranes12010097.
- Jin, P., Jiang, Z., Bao, C., Hao, S., Zhang, X., 2017. The energy consumption and carbon emission of the integrated steel mill with oxygen blast furnace. Resour. Conserv. Recycl. 117, 58–65. https://doi.org/10.1016/j.resconrec.2015.07.008.
- Katayama, K., Bahzad, H., Boot-Handford, M., Patzschke, C.F., Fennell, P.S., 2020. Process integration of chemical looping water splitting with a sintering plant for iron making. Ind. Eng. Chem. Res. 59, 7021–7032. https://doi.org/10.1021/acs. jecr.9b05045
- Khallaghi, N., Abbas, S.Z., Manzolini, G., De Coninck, E., Spallina, V., 2022. Techno-economic assessment of blast furnace gas pre-combustion decarbonisation integrated with the power generation. Energy Convers. Manag. 255. https://doi.org/10.1016/j.enconman.2022.115252.
- Kim, H., Lee, J., Lee, S., Lee, I.-B., Park, J., Han, J., 2015. Economic process design for separation of CO2 from the off-gas in ironmaking and steelmaking plants. Energy 88, 756–764. https://doi.org/10.1016/j.energy.2015.05.093.
- Kolle, J.M., Fayaz, M., Sayari, A., 2021. Understanding the effect of water on CO2 adsorption. Chem Rev 121, 7280–7345. https://doi.org/10.1021/acs.chemrev.0c00762.
- Li, Z., Yi, Q., Zhang, Y., Zhou, H., Zhao, Y., Huang, Y., et al., 2020. Numerical study and design strategy for a low emission coke oven system using oxy-fuel combustion of coke oven gas. J. Clean. Prod. 252, 119656. https://doi.org/10.1016/j. iclepro.2019.119656
- Li, R., Lian, S., Zhang, Z., Song, C., Han, R., Liu, Q., 2022. Techno-economic evaluation of a novel membrane-cryogenic hybrid process for carbon capture. Appl. Therm. Eng. 200, 117688. https://doi.org/10.1016/j.applthermaleng.2021.117688.
- Luca, A.-V., Petrescu, L., 2021. Membrane technology applied to steel production: Investigation based on process modelling and environmental tools. J. Clean. Prod. 294, 126256. https://doi.org/10.1016/j.iclepro.2021.126256.
- Luo, M., Wang, C., Yi, Y., Liu, K., Cai, J., Wang, Q., 2018. Power generation from coke oven gas using chemical looping combustion: thermodynamic simulation. Chem. Eng. Technol. 41, 524–531. https://doi.org/10.1002/ceat.201700322.
- Manzolini, G., Giuffrida, A., Cobden, P.D., van Dijk, H.A.J., Ruggeri, F., Consonni, F., 2020. Techno-economic assessment of SEWGS technology when applied to integrated steel-plant for CO2 emission mitigation. Int. J. Greenh. Gas Control 94. https://doi.org/10.1016/j.ijggc.2019.102935.
- Manzolini, G., Giuffrida, A., Zecca, N., Lücking, L., Pieterse, J.A.Z., Sebastiani, F., et al., 2022. DISPLACE technology to efficiently decarbonize steel industry. Proceedings of the 16th Greenhouse Gas Control Technologies Conference (GHGT-16).
- Martínez, I., Fernández, J.R., Abanades, J.C., Romano, M.C., 2018. Integration of a fluidised bed Ca–Cu chemical looping process in a steel mill. Energy 163, 570–584. https://doi.org/10.1016/j.energy.2018.08.123.
- https://doi.org/10.1016/j.energy.2018.08.123.
 Martínez, I., Fernández, J.R., Martini, M., Gallucci, F., van Sint Annaland, M.,
 Romano, M.C., et al., 2019. Recent progress of the Ca-Cu technology for
 decarbonisation of power plants and carbon intensive industries. Int. J. Greenh. Gas
 Control 85, 71–85. https://doi.org/10.1016/j.ijggc.2019.03.026.
- Martinez Castilla, G., Biermann, M., Montañés, R.M., Normann, F., Johnsson, F., 2019. Integrating carbon capture into an industrial combined-heat-and-power plant: performance with hourly and seasonal load changes. Int. J. Greenh. Gas Control 82, 192–203. https://doi.org/10.1016/j.iigec.2019.01.015.
- 192–203. https://doi.org/10.1016/j.ijggc.2019.01.015.
 Perpiñán, J., Peña, B., Bailera, M., Eveloy, V., Kannan, P., Raj, A., et al., 2023. Integration of carbon capture technologies in blast furnace based steel making: a comprehensive and systematic review. Fuel 336, 127074. https://doi.org/10.1016/j.
- Petrescu, L., Chisalita, D.-A., Cormos, C.-C., Manzolini, G., Cobden, P., van Dijk, H.A.J., 2019. Life cycle assessment of SEWGS technology applied to integrated steel plants. Sustainability 11. https://doi.org/10.3390/su11071825.

- Qie, Y., Lyu, Q., Lan, C., Zhang, S., 2020. Energy Conservation and CO2 Abatement Potential of a Gas-injection Blast Furnace, vol. 39, pp. 96–106. https://doi.org/ 10.1515/htmp.2020.0031
- Quader, M.A., Ahmed, S., Raja Ghazilla, R.A., Ahmed, S., Dahari, M., 2016. Evaluation of criteria for CO2 capture and storage in the iron and steel industry using the 2-tuple DEMATEL technique. J. Clean. Prod. 120, 207–220. https://doi.org/10.1016/j. iclearce.2015.10.055
- Ramírez-Santos, Á.A., Bozorg, M., Addis, B., Piccialli, V., Castel, C., Favre, E., 2018. Optimization of multistage membrane gas separation processes. Example of application to CO2 capture from blast furnace gas. J Memb Sci 566, 346–366. https://doi.org/10.1016/j.memsci.2018.08.024.
- Remus, R., Aguado-Monsonet, M.A., Roudier, S., Delgado, Sancho L., 2013. Best Available Techniques (BAT) Reference Document for Iron and Steel Production -Industrial Emissions Directive 2010/75/EU (Integrated Pollution Prevention and Control)
- Santamaría, L., Korili, S.A., Gil, A., 2023. Layered double hydroxides for CO2 adsorption at moderate temperatures: synthesis and amelioration strategies. Chem. Eng. J. 455, 140551. https://doi.org/10.1016/j.cej.2022.140551.
- Sebastiani, F., James, J., Van Dijk, E., Pieterse, J.A.Z., Boon, J., Cobden, P., 2021. Modelling of CO2 and H2O Interaction during Adsorption Cycles on Hydrotalcite for SEWGS Applications.
- Sebastiani, F., Lucking, L., Sarié, M., James, J., Boon, J., Eric van Dijk, H.J.A., et al., 2022. Steam and pressure management for the conversion of steelworks arising gases to H2 with CO2 capture by stepwise technology. Separations 9. https://doi.org/ 10.3390/separations9010020.
- Sun, Z., Liu, J., Sun, Z., 2020. Synergistic decarbonization and desulfurization of blast furnace gas via a novel magnesium-molybdenum looping process. Fuel 279, 118418. https://doi.org/10.1016/j.fuel.2020.118418.
- Tian, S., Jiang, J., Zhang, Z., Manovic, V., 2018. Inherent potential of steelmaking to contribute to decarbonisation targets via industrial carbon capture and storage. Nat. Commun. 9, 4422. https://doi.org/10.1038/s41467-018-06886-8.
- Tsupari, E., Kärki, J., Arasto, A., Lilja, J., Kinnunen, K., Sihvonen, M., 2015. Oxygen blast furnace with CO2 capture and storage at an integrated steel mill Part II: economic feasibility in comparison with conventional blast furnace highlighting sensitivities. Int. J. Greenh. Gas Control 32, 189–196. https://doi.org/10.1016/j.iigec.2014.11.007.
- van Dijk, H.A.J., Cobden, P.D., Lukashuk, L., de Water, L van, Lundqvist, M., Manzolini, G., et al., 2018. STEPWISE project: sorption-enhanced water-gas shift technology to reduce carbon footprint in the iron and steel industry. Johnson Matthey Technology Review 62, 395–402. https://doi.org/10.1595/ 205651318X15268923666410.
- Wang, Q., Luo, J., Zhong, Z., Borgna, A., 2011. CO2 capture by solid adsorbents and their applications: current status and new trends. Energy Environ. Sci. 4, 42–55. https://doi.org/10.1039/C0EE00064G.
- Wright, A.D., White, V., Hufton, J.R., Quinn, R., Cobden, P.D., Van Selow, E.R., 2011. CAESAR: development of a SEWGS model for IGCC. Energy Proc. 4, 1147–1154. https://doi.org/10.1016/j.egypro.2011.01.167.
- Xiang, D., Zhao, S., 2018. Parameter optimization and thermodynamic analysis of COG direct chemical looping hydrogen processes. Energy Convers. Manag. 172, 1–8. https://doi.org/10.1016/j.enconman.2018.07.007.
- Xie, H., Yu, Q., Zhang, Y., Zhang, J., Liu, J., Qin, Q., 2017. New process for hydrogen production from raw coke oven gas via sorption-enhanced steam reforming: thermodynamic analysis. Int. J. Hydrogen Energy 42, 2914–2923. https://doi.org/ 10.1016/j.ijhydene.2016.12.046.
- Xin, K., Boon, J., van Dijk, H.A.J., van Sint, Annaland M., 2024. Stability of potassium-promoted hydrotalcites for CO2 capture over numerous repetitive adsorption and desorption cycles. Frontiers in Chemical Engineering 6. https://doi.org/10.3389/fceng/2024.1272152
- Yang, R.T., 1997. Gas Separation by Adsorption Processes. PUBLISHED BY IMPERIAL COLLEGE PRESS AND DISTRIBUTED BY WORLD SCIENTIFIC PUBLISHING CO. https://doi.org/10.1142/p037
- Yang, F., Meerman, J.C., Faaij, A.P.C., 2021. Carbon capture and biomass in industry: a techno-economic analysis and comparison of negative emission options. Renew. Sustain. Energy Rev. 144, 111028. https://doi.org/10.1016/j.rser.2021.111028.
- Yun, S., Jang, M.-G., Kim, J.-K., 2021. Techno-economic assessment and comparison of absorption and membrane CO2 capture processes for iron and steel industry. Energy 229, 120778. https://doi.org/10.1016/j.energy.2021.120778.
- Zecca, N., Cobden, P.D., Lücking, L., Manzolini, G., 2023. SEWGS integration in a direct reduction steelmaking process for CO2 mitigation. Int. J. Greenh. Gas Control 130. https://doi.org/10.1016/j.ijggc.2023.103991.